Author response on "Case study of wave breaking with high-resolution turbulence measurements with LITOS and WRF simulations" *by* A. Schneider et al.

Review by Wayne K. Hocking

We thank the reviewer for his detailed review and for alerting us to literature that previously escaped our notice.

In the following, the review is quoted in italics part by part, and our response given below.

Part A – scientific issues

My first impression is that the paper is trying too hard to justify the idea of "being the first" on a number of fronts. It is not necessary for a paper to always "be the first", and a good paper can make meaningful contributions even if such status is not valid. In this case, I feel that the paper over-reaches in this area. It claims that, to the knowledge of the authors, "currently the only instrument for the direct in situ observation of turbulent wind fluctuations in the middle stratosphere is the balloon-borne instrument Leibniz Institute Turbulence Observations in the Stratosphere (LITOS)". Other statement pertaining to the uniqueness of the paper occur elsewhere in the text, where the authors discuss the Richardson number, and the essentially repeat the studies of Hines (1988), who introduced the idea of the "slantwise instability" as far back as 1988.

We are sorry that our phrasing was mistakable, leading to the impression of claiming to be better than we actually are. As described below, we have rewritten the introduction. The sentence under discussion regarding LITOS has been deleted. The introduction now puts our method and instrument in a better context of existing data sets from airplanes etc. Regarding the discussion about the validity of the Richardson criterion, we have now put it in a "historical" context. In fact we did not claim to be the first here, but wanted to keep the description short as this has already been described in a previous paper from our group (Haack et al, 2014). In the revised version we provide a broader discussion and proper reference of this topic inclusive the slantwise instability described by Hines.

The first measurements of velocity fluctuations in the stratosphere using balloon-borne instruments was due to Barat (1982), which the authors do refer to later, but fail to give it due recognition. More recently, extensive measurements (including velocity, temperature and humidity) have been presented by Cho et al., (Cho, J.Y.N., Newell,R.E., Anderson,B.E., Barrick,J.D.W., Thornhill,K.L., 2003, Characterizations of tropospheric turbulence and stability layers from aircraft observations.J.Geophys.Res.108(D20),8784. http://dx.doi.org/10.1029/ 2002JD0082820) and Cornman ((1) Cornman, L.B., Corrine, S.M., Cunning, G., 1995, Real-time estimation of atmospheric turbulence severity from in-situ aircraft measurements, J. Aircraft 32, 171–177.; and (2) Cornman, L.B., Meymaris, G., Limber, M., 2004, An update on the FAA Aviation Weather Research Program's in situ turbulence measurement and report system. Preprints.In:11th Conference on Aviation, Range, and Aerospace Meteorology, Hyannis, MA, Amer. Meteor. Soc. CD-ROM, P4.3.f.

None of these latter works are referenced. It also should be noted that Dehghan et al., ("Comparisons between multiple in-situ aircraft turbulence measurements and radar in the troposphere", J. Atmos. Solar-Terr. Phys., 118(A), 64-77, http://dx.doi.org/10.1016/j.jastp.2013.10.009, 2014) have found errors in the calibration of the papers by Cornman et al.

It is true that the procedures used in the paper under review are probably the most detailed I have seen, but they are not the only ones. The procedure used by Cornman and colleagues, for example, places accelerometers on commercial aircraft and measures turbulent fluctuations. The results are of course heavily

filtered because only scales comparable to and larger than the size of the aircraft are measured, which partly accounts for the corrections introduced by Dehghan et al (2014). However, the sheer magnitude of measurements by this technique is staggering, and vastly outweighs the measurements by LITOS - an important aspect for studies of large-scale diffusion, as will be discussed below. The works by Cho et al. are much more thorough.

Nevertheless, the fact remains that LITOS is not the only instrument used for these studies, nor is it the only instrument which measures velocity fluctuations.

As mentioned above, our phrasing seems to have been mistakable, thus we have revised it. However, we did not claim that LITOS is the only instrument measuring velocities in general, but that LITOS is currently the only instrument for the in-situ measurement of wind fluctuations *in the middle stratosphere*, i. e. above airplane flight altitudes. Since Barat's (1982) instrument seems to be no longer in operation, and all other in situ instruments for small-scale wind measurement known to us cannot measure in the middle stratosphere, we still think our statement is correct. We agree that the database used by Cornman et al. (1995) is much larger, but it is from commercial aircraft flying in the upper troposphere or lowermost stratosphere, not the middle stratosphere. Similarly, Cho et al. (2003) used data from aircraft with a ceiling of 8 km, i. e. tropospheric heights. In the revised introduction, we have cited Cornman et al. (1995) to point out the contrast in available data for the different heights.

There are a variety of instances when the authors do not give due recognition. The work of Barat, Sidi, Wilson etc., who have spent over 30 years studying stratospheric turbulence - mainly with temperature probes - have not been mentioned in the introduction. (see the references in Osman et al., 2016, discussed below).

So these references need to be added.

We admit that the introduction was overly short in some aspects. We have rephrased it and in this context have added some references, especially technical papers. Besides, we want to focus on wave saturation and breaking, thus we have limited the cited scientific works to those related to these topics.

However, rather than simply being critical, I would like to offer an alternative approach to the introduction. I first invite the authors to look at the introduction to Osman et al., (2016) viz. Osman, M.K., W. K. Hocking and D. W. Tarasick, "Parameterization of Large-Scale Turbulent Diffusion in the presence of both well-mixed and weakly mixed patchy layers", J. Atmos. Solar-Terr. Phys., 143-144 14-36, 2016.

[. . .]

The importance of this work to the current paper is as follows: earlier works suggested that large-scale stratospheric diffusion rates were determined by the many thousands of small layer of turbulence, whereas the work of Osman et al. suggests that it is the small number of large layers which dominate the diffusion process. The work presented in the paper under review can help resolve this critical question of how large scale diffusion relates to small-scale turbulent layering, and in so doing will have major impact on the parameterization of large-scale 2D stratospheric models - including WRF. I am not asking that the authors resolve the issue - but simply that they link their measurements to this critical debate.

A discussion along the lines given above in the introduction will strengthen the paper enormously and highlight this critical issue of the relation between localized turbulence and large-scale diffusion. Unfortunately, despite the incredible importance of this issue, it is not as widely understood as it should be, and this is an excellent chance to emphasize this issue. Bringing the issues to the forefront can of course also allow justification for more detailed research and hence raise the profile of the issue within granting agencies.

We agree that the issues of intermittency and turbulent mixing are important. LITOS data are very suitable for such a study. Yet this is outside the scope of this paper, which is about wave breaking and turbulence. We want to address these issues in future work.

[. . .]

I therefore ask that the authors substantially revise their introduction, add the references cited, discuss in more detail the work of Sidi, Wilson etc., (see references in Osman et al, 2016) and demonstrate the nature of their work within the context of this important discussion.

We have revised the introduction, setting our measurements in a better historical context. Furthermore, we have strengthened the description of the geophysical scope.

Richardson number*; First, in several places the authors discuss the relevance of the Richardson number. They conclude that this only applies in purely horizontal flows, whereas gravity waves are 3D e.g. page 6, para 2, lines 4-5 and elsewhere. They then discuss their own resolution of the problem using Achatz (2005). However, this problem was raised and discussed by Hines in 1988 (Hines, C. O., Generation of Turbulence by Atmospheric Gravity Waves, J. Atmos. Sci., 45, 1269–1278, 1988) and a citation of his work is very much deserved in this context.*

We thank the referee for pointing us to Hines (1988)'s work which has inspired many later works. We have added a few sentences mentioning his ideas:

"Already Hines (1988) discussed slantwise static instabilities created by gravity waves. He developed a wave period criterion for turbulence by comparing the e-folding time of the (slantwise) instability with the period of the wave. Turbulence is more likely to occur for slantwise static instability than for vertical static instability."

Shedding*: The authors discuss the idea that wave breaking is not due to single waves, but due to multiple waves adding together, and also the idea that the waves do not break catastrophically, but at times simply throw off just enough energy to allow them to become stable. This is a process called "shedding", or alternatively "convective adjustment", which is very well documented in the literature. The authors refer to it as "continuous fractional wave breaking" (page 11, paragraph 3). It is very important that the authors (again) give credit to those who have gone before them. References, and extensive discussion, can be found in Hocking, W.K., A review of Mesosphere–Stratosphere–Troposphere(MST) radar developments and studies, circa 1997–2008, Journal of Atmospheric and Solar-Terrestrial Physics (2010), doi:10.1016/j.jastp.2010.12.009, section 8. An even more extended discussion can be found in "Atmospheric Radar: Application and Science of MST Radars in the Earth's Mesosphere, Stratosphere, Troposphere and weakly Ionized Regions", Cambridge Press, 2016, chapter 11, section 11.2.12. (Note that Hocking was not the main person who proposed this method, but has summarized the many different papers on the technique- the authors are asked to use these to references simply as a starting point for their own clarification, and to properly cite those who have discussed the method in more detail). Another paper on a similar topic, but "tuned" to the upper troposphere and stratosphere, is Fairall, C. W., A. B. White, and D. W. Thomson, A stochastic model of gravity-wave-induced clear-air turbulence, J. Atmos. Sci., 48 , 1771–1790, 1991.*

We thank the reviewer for pointing us to the correct terminology. A literature search starting from the articles given above has yielded that "saturation" seems to be the most commonly used term for the phenomenon. Thus we have changed our manuscript accordingly.

Equation (1) and appendix A*: Equation (1) and appendix A take an interesting approach to determination of the energy dissipation rate (epsilon). The traditional method for determining epsilon is to determine structure functions, or spectra, and fit relevant Kolmogoroff functions to the inertial range portion. The introduction of the method given in equation (i) began in the early 1990's, when Luebken (a co-author on this paper), introduced it as an alternative procedure in order to help resolve an argument that developed in the literature when applications of the more traditional approach produced differences of almost an order of magnitude when applied by different authors. For details of the debate, the reader is referred to Hocking, W. K., The dynamical parameters of turbulence theory as they apply to middle atmosphere studies, Earth, Planets and Space, 51 , 525-541, 1999, but the argument was resolved by introduction of Luebken's approach. However, the paper just mentioned (Hocking) then showed that the inner-scale-approach and the traditional approach produced similar values as long as the correct constants were used. The problem arose because a group of workers incorrectly used a constant pertaining to the integrated 3-D energy spectrum, whereas the*

measurements were made using a probe passing though the turbulence in a straight line, dictating the need for a different constant (the integrated 3-D spectrum and the 1D spectrum both have a $k^{-5/3}$ spectral form, giving rise to confusion). The constant differed by a factor of 3, so the epsilon thus deduced was in error by $3^{5/3}$ times, or about 6x. Similar problems have arisen in other areas of the literature, even quite recently. The Appendix of Hocking , EPS, 1999 (given above) and appendix A of Hocking et al., (book published by Cambridge Press and discussed above) show how to use the correct constants. Further verification of these constants has been given by aircraft/radar comparisons in Dehghan et al., (2014) (reference given above). Given that the issue of the correct constants is now resolved, there is no reason why the more traditional approach should not be used - and indeed it has been used for many years by a variety of authors who HAVE used the correct constants - it is simply unfortunate that from time to time papers are published by authors who apply the wrong criteria, for reasons outlined above. The use of equation (1) in the paper under review is OK, but places significant constraints on the analysis. As the author have shown, many spectra cannot be used since they do not show a "knee" in the spectrum. It would be if interest to see how the approach using l_0 and the more traditional structure function/spectral approach (with correct constants) compare. The issue is important in view of the first item discussed in this review concerning the relation between small-scale and large-scale diffusion rates. The ability to measure epsilon using only the inertial part of the spectrum allows access to a larger data set, and the most important parameters could be argued to be the frequency of occurrence of turbulent layers, and their fraction of occupancy, while the actual strength of the turbulence within the layers might be less important for determination of large-scale diffusion. Hence the availability of more useable data allows a better contribution to studies of these fractions and statistics (see P 4, ln 4 - seems the study presented here is not ideal for determining percentages). If there is insufficient room to discuss it here, it at least seems good topic for future study, and I recommend it to the authors. If the author have already done such a study, they should cite it.

For our measurement the "traditional" method to fit the inertial range of the spectrum is not possible, because that method crucially depends on the absolute value of the periodogram, which is not available due to missing calibration. A calibration to infer wind velocities from the anemometer voltage of the constant temperature anemometer would be difficult because it has to be performed in a laboratory for known velocities under the same ambient conditions for pressure and temperature as the measurement. Conditions of a balloon flight, where pressure varies within several orders of magnitude and temperature changes by $\sim$80 K, are very difficult to simulate in a wind tunnel. We do not know a facility where such a calibration would be possible. Thus we use a variation of Lübken's method which does not need a calibration.

We agree that a comparison of dissipation rates from both retrievals, i. e. the traditional inertial range method and Lübken's method, would be very interesting. We have planned to do such a comparison for a measurement on the ground where the calibration problem can be solved with relative ease.

Use of WRF**: The authors include substantial discussions of the wave-field inferred from the WRF model. I do find myself wondering about the validity of this approach. Are modern models really good enough to reproduce the detailed small-scale structure in real-life situations? It seems somewhat unlikely to me, but perhaps I have not kept apace with current computer developments. But treating the model output as a true representation of the wind and temperature field seems a stretch. Even if the waves are generated reasonably accurately in amplitude, variations of phase estimates can significantly impact the likelihood that they break (as per the author's on comments about "continuous fractional wave breaking" and also the concepts presented by Fairall et al. discussed above). I feel the approach is interesting, but am concerned it is a bit premature. I am happy to see the process introduced, **but would ask for more commentary about its likely validity.

We agree that WRF is an idealised representation and does not reproduce reality in a perfect way. In our paper it is used to get an overview of the respective meteorological situation during the LITOS flights and to demonstrate that gravity waves occured in the vicinity of the flight tracks. Our interpretation of the model results is not based the on small-scale structures, but on the general dynamics. Obviously, in some cases (e. g. the BEXUS 12 flight) small-scale dynamics in WRF is at least qualitatively correct and produces turbulent layers that were also found prominent in our observations. There was a good agreement between observed

increase in dissipation rates and intensified TKE in the model. On the other hand, we intentionally do not investigate and interpret the many cases where LITOS observes turbulence and WRF not. All our statements derived from WRF are based on well-resolved events.

We agree that a general validation of model results was missing and have added plots of winds and temperatures from WRF interpolated along the trajectory to the plots of the radiosonde measurements. These compare very well, the only difference is that the radiosonde data contain signatures from small-scale gravity waves which WRF cannot resolve.

Part B – grammatical

We thank the referee for the detailed grammatical corrections. We appreciate the effort.

P 1, abstract, line 9 - Particularly → In particular

Changed.

P 1, ln 17 - "This typically happens in the mesosphere". What typically happen there? Are the authors talking about catastrophic wave breakdown, or shedding? As discussed in part A, wave breaking is expected in some form everywhere, either by full breakdown or multiple-wave interference effects, so I am not sure this sentence is especially useful.

We have removed this sentence in our revised version of the introduction. Instead, we have written: "This mechanism has been suggested by Hodges (1967) to explain turbulence in the mesosphere."

P 2, l1 - Measurements are → Measurements have been??

This sentence has been removed in the revision process.

P 2, ln 19 - use of "thereof" seems odd - suggest replacing with "comprising".

Changed.

P 3, ln 1 - "booms sticking out" → "booms protruding"

Changed.

P 3, ln 8 - suggest "windows of 5m" → "windows with depths of 5m"??

Changed.

P 3, ln 25 - rejection of spectra which are "not meaningful" - seems presumptive to assume that the only acceptable spectra are ones consistent with their proposed theory, though its understandable that no useful epsilon can be achieved in such circumstances I guess.

We state that if the bend in the spectrum is not resolved, the *fit* is not meaningful (not the spectrum). That means no ε can be retrieved using Heisenberg's model. We have added a phrase to clarify that:

"This means that the bend in the spectrum is not within the fit range and thus the fit is not meaningful, allowing no useful retrieval of ε."

Generally, we only consider spectra that follow the turbulence model, which may exclude turbulence that is not fully developed. The criteria sort out cases where ε cannot be retrieved. In our manuscript we have added two sentences discussing this issue:

"Requiring the spectrum to follow Heisenberg's turbulence model may exclude turbulence that is not fully developed. However, it is not feasible to retrieve ε in cases where the periodogram does not follow the turbulence model."

P 4, ln 3 - suggest "conditions" → "above conditions"

Changed.

P 4, ln 4 - suggest "rigorous criteria" → "rigorous criteria applied"

Changed.

P 4, ln 8 - "sensor has been ..." → "sensor has been located ..."

Changed.

P 4, ln 26 - reference to Hines' work on slantwise instability is needed.

Done, see response above under Part A.

P 5, ln 28 - the 30% does not seem meaningful due to the selection criteria used.

We have rephrased the sentence to make clear the 30 % is according to the criteria presented in Section 2.1:

"Overall, ∼30 % of the atmosphere was turbulent according to the criteria presented in Section 2.1."

P 6, ln 2 - "with respective phase velocities" - with respect to what? the meaning of the sentence is quite unclear.

We have rephrased the sentence as "caused filtering of gravity waves with phase velocities equal to the background winds (if present)."

P 6, ln 6 - "other side" - do you mean "other hand"?

Yes, changed.

P 6, ln 19 - "It visualizes.." → "It demonstrates..." ??

Changed.

P 8, ln 1 - could change "..at 27 Mar 2014 10:10 UT." to "..on 27 Mar 2014 at 10:10 UT."

Changed, also for the other flights.

P 8 ln 7... ".. were easterly and turned northwards ..." This is a confusing mixture of directional conventions use either ".. were westward and turned northwards.." or "were easterly and turned southerly.." Similar problems exist elsewhere in the text - try to standardize directional information (meteorological directions end in "ly" and indicate the direction from which the wind comes. whereas middle-atmosphere convention more commonly ends directions in "..ward" and indicate the direction in which the wind is blowing towards. Whichever convention is used is fine, but please try to standardize.

This was an error. Northwards has been corrected to northerly.

P 8 ln 31 - "and partly even smaller..." - do you mean "and at times smaller.." ??

Yes, changed.

P 9, ln 12 - mention is made of a "layer(ed) structure" - since it is a 1D vertical profile, how ca you be sure it is really layered?

We cannot be sure about the horizontal extension of the layers. Our use of the term "layer" stemmed from the general belief that turbulence occurs in pancake-shaped layers of a few 10 m vertical and several km horizontal extent, which is supported by radar and aircraft measurements. To avoid misunderstandings, we have changed our phrasing to "patchy structure".

P 9, ln 26 - maybe change "yields" to "suggests" ?

Changed.

P 10, paragraph 2 - while a useful summary of these data, there were only 4 flights, and these results can really only be considered as anecdotal.

A phrase was added to clarify that averages over altitude for single flights are meant.

P 10, last paragraph. Some of these references could be cited in the introduction.

All of these references except Wilson et al. (2014) are already cited in the introduction.

P 11, lines 21-22 - link to pre-existing papers regarding shedding and convective adjustment rather than introducing yet another name.

As mentioned above, we have changed the terminology to wave saturation, and have cited papers discussing it.

Anonymous Referee #2

Major comments

1. *Regarding the WRF simulations we are not given any evidence the simulations are correctly modeling the atmospheric environment. At a minimum, comparison of wind and temperature profiles at the location of the balloon ascents to the LITOS profiles should be done. And there should be plenty of surface data to compare to as well. Also, what about comparisons to satellite imagery: is there any evidence of waves in the images? If so what are the wavelengths and do they agree with the WRF predicted wavelengths?*

   We agree that a validation of our WRF simulations was missing in the manuscript. We have plotted WRF data for winds and temperatures along the LITOS ascents, which shows that WRF captures the atmospheric structures well. We have also cited the paper Ehard et al. (2016), which shows a combination of WRF simulations with lidar and radiosonde data over northern Scandinavia with nearly the same model set-up as in our paper and demonstrates the ability of WRF to properly simulate GW events. Our interpretation of the WRF data is not based on specific wave parameters. For instance, we do not extract wavelengths from WRF and the exact wavelengths are not important for our reasoning. Thus, a detailed comparison of gravity wave parameters in WRF with observations is not necessary and outside the scope of this paper.

2. *In a similar vein, while I agree that 2 km resolution is probably sufficient to resolve most gravity waves that may be generated either topographically or from other sources, it is not sufficient to model "wave breaking". This would require much higher resolutions. See e.g., Kim et al. MWR 2014 and Trier and Sharman, MWR 2016 for examples of the effects of model grid spacing on gravity wave resolutions.*

   We agree that our WRF simulations cannot simulate GW breaking of small-scale GWs with horizontal wavelengths smaller than about 10 km. Wave breaking can, however, also occur for larger-scale GWs, which are explicitely resolved by the model. Ehard et al. (2016) show regions of wave breaking at altitudes between 25 km to 30 km by means of convective overturning and reduced Richardson numbers, which was simulated by WRF with grid distances of 2 km. In our paper we use the TKE output from the model, which is provided by the boundary layer scheme and shows regions of intensified turbulent mixing in the atmosphere. For some flights (e. g., BEXUS 12, Fig. 2) these regions agree well with regions of increased dissipation rates from LITOS. Apart from that, we do not discuss turbulence that is not resolved in WRF, but observed by LITOS, since of course WRF cannot resolve all details that LITOS can measure. We added some sentences and citations about this issue in Section 2.2. Moreover, we have added a sentence at the end of Section 3.1 stating that we intentionally do not examine turbulence unresolved in WRF.

3. *Another approach might be to attempt to diagnose regions of gravity wave breaking from the LITOS or model derived soundings using standard gravity wave drag parameterizations, described e.g., in Nappo's 2002 book, and used in Kim and Chun JAMC 2011. Also looking for the presence of gravity wave critical levels in the WRF output may be useful in diagnosing regions of likely wave breaking.*

   Kim and Chun 2011 diagnosed turbulence sources for a large dataset by looking at lightning data for convective generation, reanalysis data for shear-induced turbulence from jet streams, and a digital elevation model for mountain waves. While this probably works for statistical statements as done by Kim and Chun 2011, we think it will not work for individual cases.

4. *Looking at the LITOS figures I really don't see a good correlation between epsilon and low values of Ri. This is not unexpected (e.g., Galperin et al. ASL 2007), and implies it is difficult if not impossible to assign a threshold Ri for turbulence. The authors discuss this in Section 2.1, but it should be also emphasized in the conclusions section.*

   We have added a respective paragraph in the conclusions:

   "Turbulence has been observed for Richardson numbers below as well as above the critical number of 1/4, partly even for values larger than 100. Such a violation of the classical theory by Miles (1961) and Howard (1961) has already been described by several researchers, e. g. Achatz (2005); Galperin et al. (2007); Haack et al. (2014). Hines (1988) recognised the limitation of considering only vertical instability (as done when using the Richardson number) and proposed a concept of slantwise instabilities as created by gravity waves. He showed that turbulence is more likely to develop via slanted instability. Thus turbulence for $Ri > 1/4$ is comprehensible."

Minor comments

1. *p. 2 line 27. Do you mean a precision of 1 cm s-1?*

   We mean a precision of a few cm s^{-1}.The sentence was changed accordingly.

2. *p. 3 line 6. Do you mean "sensors" instead of "sectors"?*

   Yes, changed.

3. *p. 3 lines 10-13. While I understand the attempt to use the Heisenberg spectrum to fit the high frequency end of the measurements, wouldn't it be simpler and less error prone to simply fit the portion of the spectrum in the inertial range to determine epsilon?*

   Deriving ε from fitting the inertial range of the spectrum is not possible for our measurement. For this method, the dissipation rate crucially depends on the absolute value of the periodogram, which is unknown due to missing calibration. A calibration to infer wind velocities from the anemometer voltage would be difficult because it has to be performed in a laboratory for known velocities under the same ambient conditions for pressure and temperature as the measurement. Conditions of a balloon flight, where pressure varies within several orders of magnitude and temperature changes by $\sim$80 K, are very difficult to simulate in a wind tunnel. We do not know a facility where such a calibration would be possible.

4. *p. 3 line 20. How can epsilon computed from eqn (10) ever be negative when the individual terms are raised to the 4th power and are therefore even, and nu should always by positive?*

   We thank the reviewer for pointing at this issue. The condition stems from an earlier version of our retrieval a few years back when ε was fitted instead of l_0, which numerically allowed negative values of ε to be returned by the fitting procedure (equation (1) had been incorporated in the fit function). With the changed fit parameter this is no more possible. Thus the condition can now safely be removed. In the manuscript, this item has been deleted.

5. *p. 11 line 22. Could you elaborate on what is meant by "continuous fractional wave breaking"?*

   We have changed the term to "wave saturation".

6. *In the LITOS figures (1,3,5,7), what is heating rate on the left panel? It would be interesting to plot shear and stability as well, and this may help in assessing the character of the turbulence.*

   On the right panel, the top axis gives the heating rate due to turbulent dissipation, $\mathrm{d}T/\mathrm{d}t = \varepsilon/c_p$. A sentence was added in the figure caption to explain that:
   "The top axis gives the heating rate due to turbulent dissipation, $\mathrm{d}T/\mathrm{d}t = \varepsilon/c_p$."

   Since the Richardson number does not correspond well to turbulence (cf. major comment 4), splitting *Ri* in wind shear and buoyancy frequency seems not to provide useful information.

7. *Appendix. The gamma function in the eqns is not defined.*

   A phrase defining it was added:
   "where [...] $\Gamma(z) := \int_0^\infty t^{z-1}\mathrm{e}^{-t}\,\mathrm{d}t$ is the Gamma function, ..."

Anonymous Referee #3

Major comments

- *The main point made by the authors is that an increase in GW breaking is associated to the increase in turbulence dissipation. If the authors mean that high GW* leads *to stronger turbulence, I agree. But the I would be cautious to generalize this statement implying (as the authors say at the end of Conclusions), that turbulence in the atmosphere is generated by continuous GW activity because the latter is only* one *of the causes triggering turbulence in the atmosphere (other drivers are large-scale convention, shear instabilities, etc. which do not necessarily involve GW).*

  We mean that high GW leads to stronger turbulence. This is seen in our measurements by large dissipation for large GW amplitudes and low dissipation for small GW amplitudes. Of course, other sources could contribute to turbulence as well when present. At the end of our conclusions, we have removed the word "generally" which may have been mistakable, i. e. the sentence now reads:
  "Altogether, observed dissipation is weaker during lower wave activity (as seen in WRF), and larger where larger wave amplitudes are seen."

- *I do not believe that WRF can provide reliable information on turbulence characteristics in the chosen simulation set-up, at least the authors didn't show substantial evidence it can. The main is reasons is of course the coarse resolution: 2 km is not even close to resolve eddies in a substantial (and potentially relevant to observational data) portion of the inertial range, should turbulence develop following GW breaking. Indeed, the discussion on the simulation results rely entirely on the supposed correctness of the modeled TKE transport rather than the resolution of turbulent scales! In addition, there are no details on the TKE parameterization used in the runs so it is not clear whether such parametrizing is correctly tailored to the cases analyzed. There's a huge literature on DNS/LES modeling of turbulent stratified flows -which apply to atmospheric turbulence as wll- discussing these issues. You can refer to the review study by Brethauwer et al, JFM 2007 and to more recent works such as Kani and Waite, JFM 2014, and Paoli et al, ACP 2014 in addition to the work by Fritts and coworkers on GW breaking that you cited.*

  We agree that our WRF simulations cannot simulate GW breaking of small-scale GWs with horizontal wavelengths smaller than about 10 km. Wave breaking can, however, also occur for larger-scale GWs, which are explicitely resolved by the model. Ehard et al. (2016) show regions of wave breaking at altitudes between 25 km to 30 km by means of convective overturning and reduced Richardson numbers,

which was simulated by WRF with grid distances of 2 km. In our paper we use WRF to get an overview of the meteorological situation and to detect regions along the balloon ascent, where increased subgrid-scale turbulent diffusion (increased TKE) was simulated by means of the boundary layer scheme. This scheme is described in Nakanishi and Niino (2009). We added some additional sentences and citations about this issue in Section 2.2.

- *I agree with your consideration on Richardson number and the difficulty to match the theoretical Ri=0.25 threshold for shear instability in real atmospheric situations. To support your discussion, you may also refer to the work by Paoli et al, ACP 2014 where they used high- resolution LES (with grid sizes of order of meters) to study atmospheric turbulence at the tropopause level. They observed similar trend of Ri as a function of altitude (ex their Figs. 9- 10), and discussed the impact of turbulence intensity and the sensitivity to resolution, which can also apply to the measured profiles shown in your Fig 1c, 3c etc.*

  We agree that the vertical resolution has an impact on the Richardson number. Usually, a larger vertical resolution (i. e. smaller scales resolved) yields locally smaller *Ri* because for lower resolution *Ri* is potentially averaged over regions with low and high *Ri*. This has already been examined, e. g., by Balsley et al. (2008) and Haack et al. (2014). We have added a few sentences in our manuscript discussing this issue:
  "It should be kept in mind that the Richardson number depends on the scale on which it is computed (e. g. Balsley et al., 2008; Haack et al., 2014). A higher resolution (i. e. computing *Ri* on smaller scales) may result in locally smaller *Ri* numbers, because the computation on large scales yields a kind of average. Similarly, Paoli et al. (2014) found in LES simulations larger Richardson numbers for smaller model resolutions (i. e. larger scales). Here, due to measurement noise a smoothing over 150 m has been applied before computing *Ri*, determining the resolution. However, this issue cannot explain the whole discrepancy. Haack et al. (2014) examined the impact of the scale on which *Ri* is computed on the relation between small Richardson numbers and turbulence. They found many turbulent patches for $Ri > 1$ even even when computing *Ri* on a scale of 10 m."

- *It would very much benefit to the paper showing turbulence spectra or structure functions, particularly in the inertial range, and especially for the cases of developed turbulence where an inertial range should be neatly detected.*

  Examples of anemometer voltages and corresponding spectra for the LITOS retrievals are shown in previous papers, e. g. Theuerkauf et al. (2011); Haack et al. (2014); Schneider et al. (2015). Since in principle we use the same retrieval, these are not shown again.

Minor comments

- *What is the reason for adding a legend of K/d in addition to W/kg in the dissipation profiles of Figures 1d, 3d, etc? In fact, I also found a little weird to label the units of dissipation rate as W/kg instead of m^2/s^3 or cm^2/s^3 which is more customary in turbulence literature.*

  In some communities it is usual to give dissipation rates as heating rates in K/d, which are connected via $\mathrm{d}T/\mathrm{d}t = \varepsilon/c_p$; thus we have added this scale as second axis. W/kg is the same as $\mathrm{m}^2/\mathrm{s}^3$.

Case study of wave breaking with high-resolution turbulence measurements with LITOS and WRF simulations

Andreas Schneider[1], Johannes Wagner[2], Jens Söder[1], Michael Gerding[1], and Franz-Josef Lübken[1]

[1]Leibniz Institute of Atmospheric Physics at the University of Rostock (IAP), Kühlungsborn, Germany
[2]German Aerospace Center (DLR), Institute of Atmospheric Physics (IPA), Wessling, Germany

Correspondence to: Andreas Schneider (schneider@iap-kborn.de)

Abstract. Measurements of turbulent energy dissipation rates obtained from wind fluctuations observed with the balloon-borne instrument LITOS (Leibniz-Institute Turbulence Observations in the Stratosphere) are combined with simulations with the Weather Research and Forecasting (WRF) model to study the breakdown of waves into turbulence. Four flights from Kiruna (68° N, 21° E) and from Kühlungsborn (54° N, 12° E) are analysed. Average dissipation rates are in the order of 1 mW kg^{-1} (∼0.1 K d^{-1}) with typically higher rates in the stratosphere compared to the troposphere. During two flights energy dissipation rates strongly decreased above the tropopause. One of these cases featured a patch with highly increased dissipation directly below the tropopause collocated with shear generation and wave filtering conditions. The second case showed nearly no turbulence at all above 15 km. For the other two flights, dissipation rates increased continuously across the whole ascent. For all flights, observed energy dissipation rates are related to wave patterns visible in the modelled vertical winds. ParticularlyIn particular, the drop in turbulent fraction for two of the flights mentioned above coincides with a drop in amplitude in the wave patterns visible in WRF. For other flights both dissipation rates and wave amplitudes show continuous distributions with height. This indicates small-scale partial wave breakingwave saturation.

1 Introduction

Gravity waves transport energy and momentum and are thus an important factor in the atmospheric energetics. Typically, they are excited in the troposphere and propagate upwards and horizontally. Due to decreasing density, the amplitudes increase with altitude in the absence of damping. Eventually, the waves become unstable and break, producing turbulence and dissipation, and thereby depose their energy and momentum. This typically happens in the mesosphere. This mechanism has been suggested by Hodges (1967) to explain turbulence in the mesosphere. However, some waves already break in the stratosphere in spite of the stable stratification, e. g., at local instabilities due to wind shear. This modifies the energy flux from the troposphere to the mesosphere. A breaking wave is not always completely annihilated, but it may lose amplitude by transferring energy to smaller scales and eventually turbulence in a highly non-linear process (e. g. Franke and Collins, 2003). There are two variants of wave breaking (e. g. Hocking, 2011, Section 9): First catastrophic wave breaking, where the wave is completely annihilated (e. g. Andreassen et al., 1994), and second wave saturation, where a wave loses energy to turbulence so that the amplitude does not increase further, i. e. the wave breaks only partially (e. g. Lindzen, 1981). Hines (1991) defines saturation to

imply that the wave amplitude is at a maximum and the excess energy is shed by physical processes to prevent further growth. There are several theories for saturation (Fritts and Alexander, 2003, Section 6.3), and the phenomenon has been observed as well. For example, using a balloon-borne instrument Cot and Barat (1986) measured a gravity wave in winds and temperature with vertical wavelength of ∼1 km and nearly constant amplitude over ∼5 km height. Simultaneously they observed several turbulent patches collocated with negative temperature gradient and Richardson numbers between 0.3 and 6. They conclude that clear air turbulence is related to a long-period wave via shear instability, and that the energy budget of the wave-turbulence interaction is in an order of magnitude that the wave amplitude would not change much. Franke and Collins (2003) observed gravity waves in the mesosphere with Na lidar and found upwards propagating waves still present (with less amplitude) above an overturning region. Catastrophic wave breaking has been observed, e. g., in the lowermost stratosphere by Worthington (1998) and Pavelin et al. (2001) with radar and radiosonde. Model studies of breaking gravity waves have, e. g., been carried out by Achatz (2005) and by Fritts and Wang (2013), Fritts et al. (2016), who performed direct numerical simulations (DNS) of a gravity wave superposed by fine-scale shear.

The amount of energy deposited in the stratosphere by turbulent dissipation is largely unknown. A main reason is technical difficulties for measurements. The length scale where most dissipation occurs, also called the inner scale of turbulence l_0, is on the order of centimetres (or smaller) at stratospheric heights (e. g. Theuerkauf et al., 2011). This makes the direct observation technically challenging. For that reason, studies of stratospheric turbulence are sparse.

Regarding turbulence measurements, a relatively extensive dataset exists for the troposphere and tropopause region (e. g. Lilly et al., 1974; Hauf, 1993; Cho et al., 2003), but in the middle stratosphere observations are sparse. Remote sensing is mainly performed by radars in the troposphere and lower stratosphere as well as in the mesosphere (see Wilson, 2004, for an overview), and with satellites in the upper stratosphere (e. g. Gavrilov, 2013). In situ observations in the middle stratosphere have been carried out with balloon-borne instruments. Pioneering work has been done by Barat (1982) and Dalaudier et al. (1994). An instrument with a similar anemometer has been developed by Yamanaka et al. (1985). Indirect measurements using the Thorpe method were performed by Luce et al. (2002); Clayson and Kantha (2008) and others, mainly using standard radiosondes. A recent high-resolution balloon-borne instrument for the direct measurement of turbulent wind fluctuations is Leibniz Institute Turbulence Observations in the Stratosphere (LITOS) (Theuerkauf et al., 2011), which can resolve the inner scale of turbulence in the stratosphere for the first time. This state of the art instrument is used for this study.

Measurements are performed in the lower stratosphere with radars (see Wilson, 2004, for an overview) and aircraft (e. g. Lilly et al., 1974; Hauf, 1993), in the lower and middle stratosphere with balloons (e. g. Barat, 1982; Theuerkauf et al., 2011), and in the middle and upper stratosphere with satellites (e. g. Gavrilov, 2013). In situ techniques have the advantage of much higher precision and resolution. To our knowledge, currently the only instrument for the direct in situ observation of turbulent wind fluctuations in the middle stratosphere is the balloon-borne instrument Leibniz Institute Turbulence Observations in the Stratosphere (LITOS).

Wave breaking has been observed, e. g., in the lowermost stratosphere by Worthington (1998) and Pavelin et al. (2001) with radar and radiosonde. Plougonven et al. (2008) report mountain wave breaking over the Antarctic Peninsula. Franke and Collins (2003) observed gravity waves in the mesosphere with Na lidar and found upwards propagating waves still present

(with less amplitude) above an overturning region. Model studies of breaking gravity waves have, e. g., been carried out by Achatz (2005) and by Fritts and Wang (2013), Fritts et al. (2016), who performed direct numerical simulations (DNS) of a gravity wave superposed by fine-scale shear.

To study wave breaking into turbulence, a wide range of scales from kilometres (the wavelength of GWs) to millimetres (the viscous subrange of turbulence) has to be resolved. This cannot be performed by a single instrument. Thus several techniques have to be combined. In this study, LITOS is used for the turbulence part and radiosonde observations from the same gondola for local atmospheric background conditions. To put the observations into a geophysical context and to obtain information about waves, regional model simulations with WRF (Weather Research and Forecasting model) driven by reanalysis data are applied. Four flights are analysed, thereofcomprising two from Kiruna (northern Sweden, 67.9° N, 21.1° E) and two from Kühlungsborn (northern Germany, 54.1° N, 11.8° E).

This paper is structured as follows: Section 2 gives an overview of the instrument LITOS and the data retrieval (Section 2.1) as well as the WRF model setup (Section 2.2). The results for four different flights are presented in Section 3. These are interrelated and discussed in Section 4, and finally conclusions are drawn in Section 5.

2 Instrumentation and model

2.1 Balloon-borne measurements

LITOS (Leibniz-Institute Turbulence Observations in the Stratosphere) is a balloon-borne instrument to observe small-scale fluctuations in the stratospheric wind field (Theuerkauf et al., 2011). The wind measurements are performed with a constant temperature anemometer (CTA) which has a precision of a few $\mathrm{cm\,s^{-1}}$. It is sampled with 8 kHz yielding a sub-millimetre vertical resolution at $5\,\mathrm{m\,s^{-1}}$ ascent rate. Thus the inner scale of turbulence is typically covered. A standard meteorological radiosonde (Vaisala RS92 or RS41) is used to record atmospheric background parameters. LITOS was launched three times as part of a ∼120 kg payload from Kiruna (67.9° N, 21.1° E) within Balloon Experiments for University Students (BEXUS) 6, 8 and 12 in 2008, 2009 and 2011, respectively (Theuerkauf et al., 2011; Haack et al., 2014; Schneider et al., 2015). The second generation of the small version of the instrument is an improvement of the one described by Theuerkauf et al. (2011) and consists of a spherical payload of ∼3 kg weight. It is suspended ∼180 m below a meteorological rubber balloon. Two CTA sensors are mounted on booms sticking outprotruding at the top of the gondola. The instrument was launched several times from IAP's site at Kühlungsborn (54.1° N, 11.8° E), e. g. at 27 Mar 2014, 06 Jun 2014, and 12 Jul 2015.

In this paper, only flights are taken into account where data from more than one CTA sensor on the same gondola are available. Summarised, the data analysis is performed in three steps. First, the dissipation rate is retrieved similar as described by Theuerkauf et al. (2011). Then the ε values from both sensors are compared to detect sections where one sensor is possibly affected by the wake of ropes. Finally, the remaining spectra are manually inspected to sort out cases were both sectorssensors potentially have been in the wake.

The details of the retrieval are as follows: The data of the ascent is split into windows with depths of 5 m altitude with 50 % overlap. In each window, the mean value is subtracted, and the periodogram is computed, which is an estimation of the

power spectral density (PSD). The periodogram is smoothed with a Gaussian-weighted running average. The instrumental noise level is detected and subtracted. Initially, turbulence is assumed in each window and thus the Heisenberg (1948) model for fully developed turbulence in the form given by Lübken and Hillert (1992) and Theuerkauf et al. (2011) is tried to fit to the observed spectrum (cf. Equation (A3) in Appendix A). If the fit succeeds, the inner scale l_0 is obtained. This leads to the energy dissipation rate ε given by

$$\varepsilon = c_{l_0}^4 \frac{\nu^3}{l_0^4}, \tag{1}$$

where ν is the kinematic viscosity (known from the radiosonde measurement) and c_{l_0} is a constant depending on the type of sensor. The determination of c_{l_0} for our sensor configurations is described Appendix A. Non-turbulent (or disturbed) spectra manifest in bad fits which are sorted out with the following set of criteria:

- The noise level detection fails, which usually means that the noise is not white, i. e. the periodogram is disturbed at small scales.
- ε is negative; this may occur in very seldom cases when the spectrum is severely disturbed due to spurious effects.
- The mean logarithmic difference between data and fit exceeds a given threshold. This condition captures cases where the fit does not describe the data well, e. g. when no turbulence is present so that the periodogram does not follow form of the turbulence model.
- The inner scale l_0 lies outside the fit range. This means that the bend in the spectrum is not within the fit range and thus the fit is not meaningful, allowing no useful retrieval of ε. That can occur when the spectrum does not have the expected form of the turbulence model, when the inner scale lies at very small scales where the periodogram is dominated by noise, or when the periodogram is disturbed.
- The fit width is smaller than a threshold; in this case the fit is determined by too few data points.
- The value of the periodogram at l_0 is too close to the value of the noise level, i. e. too small a part of the viscous subrange is resolved.
- The slope of the fit function at the small-scale end is less than a given threshold (less steep than m^{-4}, where m is the vertical wave number). This indicates that the bend in the spectrum is not well covered by the fit and the data.

If one of the above conditions applies, the spectrum does not follow the form for fully developed turbulence, thus ε is set to zero. Requiring the spectrum to follow Heisenberg's turbulence model may exclude turbulence that is not fully developed. However, it is not feasible to retrieve ε in cases where the periodogram does not follow the turbulence model. Due to the rigorous criteria applied the amount of detected turbulence can be considered a lower limit. Depending on the individual profile, between 15 % and 62 % of the spectra of the single sensor profiles are classified as turbulent. Both sensors simultaneously yield turbulence for 12 % to 33 % of all data bins, depending on the flight. For the BEXUS flights much more turbulence is detected than for the flights with the small payload.

Sometimes a sensor has been located in the wake of a rope supporting the gondola and the other sensor not, causing the ε values of both sensors to differ by up to 5 orders of magnitude. To sort out such sections, altitude bins where the dissipation rate from both sensors deviates by more than a factor of 15 are discarded, which amounts to roughly 8 % to 39 % of the valid spectra depending on the individual flight.

For the flights with the small payload, the remaining spectra have been inspected manually for sections where both sensors have been affected by the wake, and those that look suspicious have been taken out. A spectrum is regarded as wake-affected if it has a plateau in PSD near 10 cm spatial scale, which is estimated to be the extent of a Kármán vortex street originating from the lines supporting the gondola. In this step, 62 of 1433 (113 of 975) spectra have been manually discarded for the flights from 27 Mar 2014 (12 Jul 2015), mainly in the troposphere and not above ∼20 km. This problem does not occur for the BEXUS flights, where the sensors were placed further away from the supporting lines. For all other altitude bins the average of both sensors is taken.

To quantify the stability of the atmosphere, the gradient Richardson number $Ri = N^2/S^2$ is used, which is the ratio of the squared Brunt-Väisälä frequency N^2 and the square of the vertical shear of the horizontal wind S^2. The Brunt-Väisälä frequency can be written as $N^2 = \frac{g}{\Theta}\frac{\mathrm{d}\Theta}{\mathrm{d}z}$, where Θ is the potential temperature and g the acceleration due to gravity. The wind shear is defined as $S^2 = \left(\frac{\mathrm{d}u}{\mathrm{d}z}\right)^2 + \left(\frac{\mathrm{d}v}{\mathrm{d}z}\right)^2$, where u and v are the zonal and meridional wind components, respectively. The Richardson number represents the ratio of buoyancy forces (which suppress turbulence) to shear forces (which generate turbulence). According to a theory for plane-parallel flow established by Miles (1961) and Howard (1961), turbulence occurs below a critical Richardson number of $Ri_\mathrm{c} = 1/4$. The general applicability of that criterion was recently questioned based on measurements (e. g. Haack et al., 2014) and model simulations (e. g. Achatz, 2005). Often the shear is not strictly horizontal so that the theory by Miles (1961) and Howard (1961) is not applicable, as pointed out by Achatz (2005). To take into account slanted shear, Hines (1988) proposed a concept of slantwise instability. However, itthe Richardson number is still useful as an estimation of stability. The Richardson number also depends on the scale on which it is computed (Balsley et al., 2008; Haack et al., 2014). Usually, computing *Ri* on a smaller scale yields locally smaller numbers, since for a computation on larger scales an average over regions with small and large *Ri* is obtained. In this study *Ri* is retrieved from the radiosonde measurements. In order not to dominate the derivatives by instrumental noise, the potential temperatures and winds are smoothed with a Hann-weighted running average over 150 m prior to differentiation with central finite differences.

2.2 Model simulations

Mesoscale numerical simulations are performed with the Weather Research and Forecasting (WRF) model, version 3.7 (Skamarock et al., 2008). Two nested domains with horizontal resolutions of 6 km and 2 km and time step 15 s and 5 s, respectively, are applied. In the vertical direction 138 terrain following levels with stretched level distances of 80 m near the surface and 300 m in the stratosphere are used and the model top is set to 2 hPa (about 40 km altitude) for the BEXUS flights and 5 hPa (about 32 km altitude) for the flights from Kühlungsborn. At the model top a 7 km thick Rayleigh damping layer is applied to prevent wave reflections (Klemp et al., 2008), i. e. the top of the damping layer is the model top. Physical parametrisations contain the Rapid Radiative Transfer Model longwave scheme (Mlawer et al., 1997), the Goddard shortwave scheme (Chou

and Suarez, 1994), the Mellor-Yamada-Nakanishi-Niino boundary layer scheme (Nakanishi and Niino, 2009), the Noah land surface model (Chen and Dudhia, 2001), the WRF single-moment 6-class microphysics scheme (WSM6; Hong and Lim, 2006) and the Kain-Fritsch cumulus parametrisation scheme (Kain and Fritsch, 1990). The initial and boundary conditions are supplied by ECMWF (European Centre for Medium-Range Weather Forecasts) operational analyses on 137 model levels with a temporal resolution of 6 hours. In WRF a temporal output interval of 1 hour is used, data interpolated along the flight track are output with an interval of 5 minutes. Simulations are initialised 5 to 6 hours before the launch time of the balloon. The computation of turbulent kinetic energy (TKE) is done by the boundary layer scheme and described in Nakanishi and Niino (2009). It is is based on a prognostic equation which is solved additionally to the equations of motion and which includes transport, shear production, buoyancy production and dissipation terms. Shear and buoyancy terms include deformation and stability effects of the resolved flow and are related to turbulent motions by the horizontal and vertical eddy viscosities. The equation operates on the scale of the grid size. WRF Simulations are initialised 5 to 6 hours before the launch time of the balloon.

In this paper WRF simulations are used to get an overview of the meteorological situation. Ehard et al. (2016) showed that regions of GW breaking can be simulated by WRF simulations with horizontal grid distances of 2 km and a similar model set-up by means of convective overturning and reduced Richardson numbers. Here, the TKE output from the model is also used to identify regions of intensified turbulent mixing in the atmosphere along the balloon flight tracks. This can be a hint that observed turbulence was caused by large-scale GW breaking. It is not intended to quantitatively compare observed dissipation rates with simulated regions of enhanced TKE values.

3 Results

3.1 The BEXUS 12 flight (27 September 2011)

The BEXUS 12 flight was launched from Kiruna aton 27 Sep 2011, at 17:36 UT. The two left panels of Figure 1 show atmospheric conditions as observed by the radiosonde on board the payload. Temperatures decreased up to the tropopause at 10.3 km, excepting some small inversion layers. Above there was a sharp increase in temperature known as tropopause inversion layer (TIL) (Birner et al., 2002; Birner, 2006). Higher up, temperatures slightly decreased. Winds came from northwest near the surface and reversed between ∼6 km and 10 km. The reversal caused nearly opposite wind direction at 9 km altitude compared to 5 km, and a change of sign in both wind components. It further entailed strong wind shear below the tropopause, causing low Richardson numbers (below the critical number of 1/4). Above the tropopause the wind field showed signatures of gravity wave activity with short wavelengths and no obvious altitude-dependent structure. In the stratosphere, Richardson numbers were generally larger than in the troposphere.

The right panel of Figure 1 depicts observed dissipation rates. Each blue cross corresponds to an altitude bin classified as turbulent (as described in Section 2.1). Overall, ∼30 % of the atmosphere was turbulent according to the criteria presented in Section 2.1. The orange curve depicts a Hann-weighted running average over 500 m. Please note that especially in the stratosphere there are various bins with $\varepsilon = 0$ which contribute to the running average but do not show up in the scatter plot. Dissipation rates varied over several orders of magnitude within only small altitude ranges (typically a few 10 m). This represents

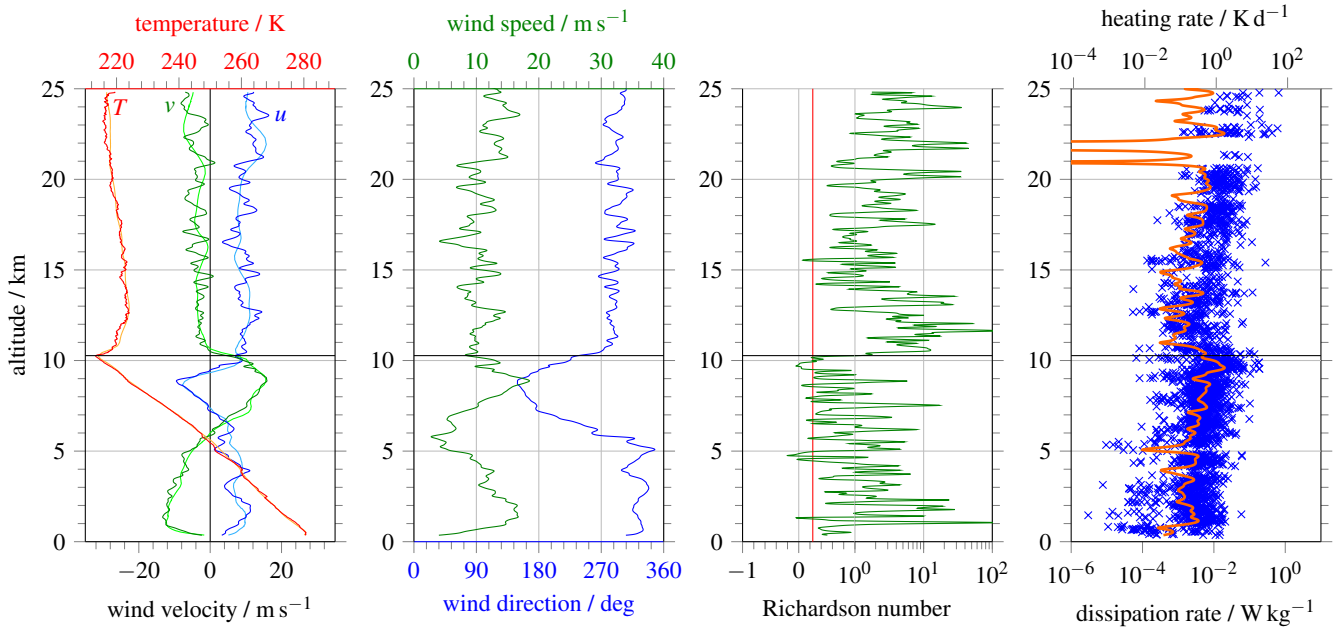

Figure 1. Observations during the BEXUS 12 flight. Left: Zonal winds u (blue), meridional winds v (green) and temperatures T (red) from the radiosonde. The light blue, light green, and orange curves show the corresponding results from the WRF model interpolated along the balloon trajectory. Centre left: Wind direction (blue) and horizontal wind speed (green) from the radiosonde. Centre right: Richardson number Ri computed from the radiosonde data, using a smoothing over 150 m prior to differentiation. The Ri axis is split at 1 into a linear and a logarithmic part. The red line shows the critical Richardson number 1/4. Right: Energy dissipation rates ε observed by LITOS. The blue crosses mark single turbulent spectra computed on a 5 m grid with 50 % overlap, the orange curve shows a Hann-weighted running average over 500 m (non-turbulent bins count as zero in the average). The top axis gives the heating rate due to turbulent dissipation, $\mathrm{d}T/\mathrm{d}t = \varepsilon/c_p$. The horizontal black line in all four panels marks the tropopause.

the well-known intermittency of turbulence. Mean dissipation rates were 2.7 mW kg^{-1} in the troposphere and 3.5 mW kg^{-1} in the stratosphere (excluding 1 km above and below the tropopause). Between 9 km and 10 km there was a thick layer with enhanced dissipation. As described above, this altitude region featured low Richardson numbers caused by high wind shears. Thus turbulence was presumably induced by dynamic instability. Additionally, at this altitude a wind reversal was observed which caused filtering of gravity waves with respective phase velocities equal to the background winds (if present). On the large scale, dissipation rates evinced an overall tendency to rise with altitude (cf. orange curve), excepting a step to smaller rates at the tropopause. For this step, two superposing causes are visible: (1) enhanced stability in the TIL, and (2) the potential gravity wave filtering indicated by the wind shear below the tropopause mentioned earlier, which means that above less waves persist that can break and produce turbulence. On the other sidehand, the wind shear is also expected to have generated new gravity waves, but these are expected to have small amplitudes.

Particularly in the stratosphere, turbulence occurred also for high Richardson numbers, in contradiction to the theory that $Ri \leq Ri_c = 1/4$ is necessary for turbulence. This behaviour is consistent with observations by Haack et al. (2014). It should be kept in mind that the Richardson number depends on the scale on which it is computed (e. g. Balsley et al., 2008; Haack et al., 2014). A higher resolution (i. e. computing Ri on smaller scales) may result in locally smaller Ri numbers, because the computation on large scales yields a kind of average. Similarly, Paoli et al. (2014) found in LES simulations larger Richardson numbers for smaller model resolutions (i. e. larger scales). Here, due to measurement noise a smoothing over 150 m has been applied before computing Ri, determining the resolution. However, this issue cannot explain the whole discrepancy. Haack et al. (2014) examined the impact of the scale on which Ri is computed on the relation between small Richardson numbers and turbulence. They found many turbulent patches for $Ri > 1$ even even when computing Ri on a scale of 10 m. In simulations of gravity waves, Achatz (2005) found instabilities and onset of turbulence for Richardson numbers both smaller and larger than 1/4. He noted that the theory by Miles (1961) and Howard (1961) is not applicable to his simulations because the gravity wave phase propagation and thus the wave-induced shear is slanted. In the light of this comment, and taking into account that iIn the real atmosphere waves usually propagate inclined (i. e. the shear is not orthogonal to the altitude axis)., Already Hines (1988) discussed slantwise static instabilities created by gravity waves. He developed a wave period criterion for turbulence by comparing the e-folding time of the (slantwise) instability with the period of the wave. Turbulence is more likely to occur for slantwise static instability than for vertical static instability. In the light of these comments, the violation of the Richardson criterion for the LITOS measurements is comprehensible.

Figure 2 depicts results from WRF model simulations were performed for the time and place of the flight. To show that these produced reasonable results, model winds and temperatures interpolated along the flight trajectory are plotted in the left panel of Figure 1 along with the radiosonde profiles. Observed and modelled results compare very well, the only difference is that the radiosonde data contain signatures from small-scale gravity waves which WRF cannot resolve. In Figure 2, model(more precisely, snapshots at the middle of the ascent are shown). The upper left panel depicts horizontal winds at 850 hPa. Westerly winds flowed over the Scandinavian mountains which are expected to have excited mountain waves. Another potential source of gravity waves is geostrophic adjustment. Bending stream lines are visible, e. g., over the Scandinavian mountains, west of the flight track. The upper right panel presents a vertical section of horizontal winds and potential temperatures. It visualisesdemonstrates that the jet ($\sim$7 km to 10 km altitude) had a local structure and involved strong wind shears.

With a grid resolution of 2 km WRF can resolve waves with horizontal wavelengths larger than about 10 km. These waves can be seen, e. g., in the vertical winds, which are used as a proxy. This quantity is plotted in the lower left panel of Figure 2. Strong wave-like patterns are visible especially over the Scandinavian mountains, which correspond to the mountain wave excitation mentioned above. Weaker wave patterns are visible near the flight trajectory, downstream of the mountains. Between roughly $x = 400$ km and $x = 550$ km, the wave patterns change at tropopause height (approximately 10 km altitude): Above there is less amplitude than below. This is ascribed to the wave breaking and filtering mentioned before. Filtering means catastrophic breaking of waves, i. e. a wave that is filtered is annihilated. Further upwards the amplitude increases slowly.

Waves can propagate over considerable distances and times. Therefore it is not sufficient to look at potential sources in the vicinity of the flight track. Even if sources are found, the waves may have propagated to other places (away from the point of

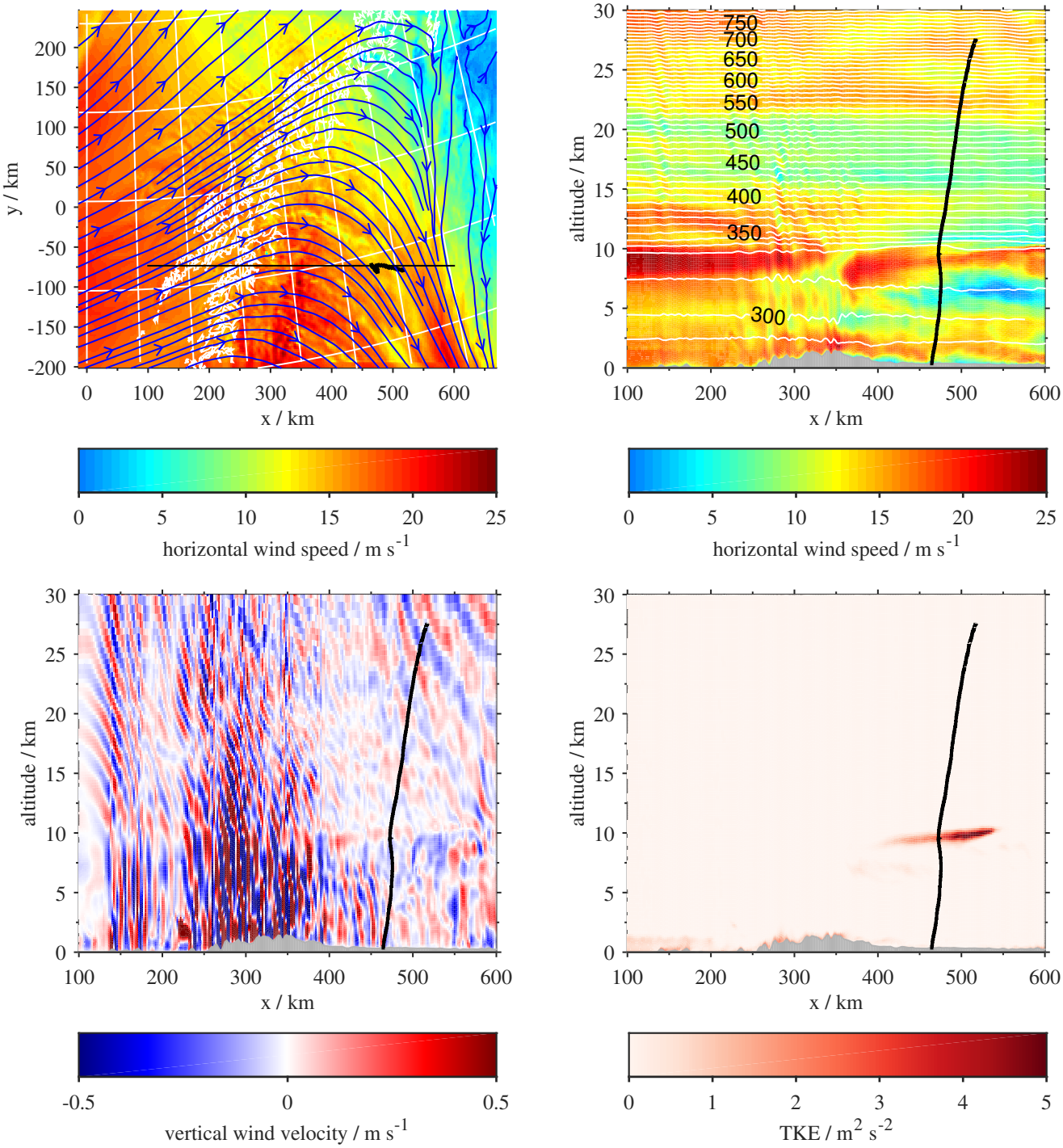

Figure 2. Map of horizontal winds at 850 hPa (upper left), vertical section of horizontal winds (upper right), vertical section of vertical winds (lower left), and vertical section of turbulent kinetic energy (TKE) (lower right) from WRF simulations for 27 Sep 2011, 18:00 UT. The black curves visualise the trajectory of the BEXUS 12 flight. In the upper left panel, the blue streamlines show the wind direction, the white lines visualise coastlines and a latitude/longitude grid, and the black line indicates the location of the vertical sections. In the upper right panel, the white isolines show potential temperature.

interest), while waves from sources outside the domain may have propagated to the location of observation. For resolved waves the model takes care of these issues. Waves seen in WRF at the location of the flight may have travelled from remote places, yet the important information is not their origin, but that they were present during the measurement.

To trigger turbulence, wave *breaking* is necessary. Such events are triggered by dynamic or convective instabilities or by wave-wave interactions (e. g. Fritts and Alexander, 2003). In WRF, the break-down to turbulence is parametrised by solving a prognostic equation for turbulent kinetic energy (TKE), which is based on production terms due to shear and buoyancy obtained from the resolved flow. TKE is plotted in the lower right panel of Figure 2. It peaks near 10 km height at the location of the flight. This corresponds nicely to the intense turbulent layer observed by LITOS. It is reproduced in WRF due to the shear instability on scales resolved by the model. That highlights the geophysical significance of that layer. With LITOS, weaker turbulence is observed over the whole altitude range (i. e. below 10 km as well as above). This background turbulence is not covered by the model, because it is caused by shear and buoyancy instabilities of the mean flow on scales smaller than resolved by the model. In the stratosphere, some layers are present with dissipation rates in similar order as observed near 10 km height, but these are relatively thin and are not associated with $Ri < 1/4$. For example, there is a layer with large dissipation rates between ∼22.48 km and 22.63 km altitude, but it is only ∼150 m thick, and Richardson numbers are around 1. In the stratosphere, the vertical model resolution is 300 m. Thus it is reasonable that the layer at 22.5 km is not reproduced in WRF with enhanced TKE. An investigation of turbulence unresolved in WRF is outside the scope of this paper, and would require a higher resolution of the model.

3.2 The BEXUS 8 flight (10 October 2009)

LITOS was previously flown on BEXUS 8, launched from Kiruna aton 10 Oct 2009, at 08:03 UT. Haack et al. (2014) already describe some features of that flight, mainly statistics about turbulent layers as well as dissipation rates and their relation to Richardson numbers. Please note that they computed dissipation profiles with a 25 m window, while here a 5 m window, an updated value of the constant c_{l_0} in (1), and an updated set of quality criteria is used. Here, the focus lies on the comparison with other flights and WRF simulations.

Figure 3 presents the observations. The temperature structure from the radiosonde data shows a tropopause at 8.1 km, i. e. considerably lower than for BEXUS 12, and only small local sections with increasing temperature above. Winds came from north western directions below ∼20 km and from south west above. No zonal wind reversal as for BEXUS 12 was present.

Energy dissipation rates are plotted in the right panel of Figure 3. Again ε is intermittent. In contrast to BEXUS 12, no pronounced maximum in dissipation is visible. This is consistent with the absence of a wind reversal or large wind shear. Richardson numbers are variable; mostly values are much larger than the critical number 1/4 in the entire troposphere and stratosphere, only some small layers with $Ri < 1/4$ are present. There is no extended region with $Ri < 1/4$ as for BEXUS 12 near 10 km altitude. Average dissipation rates are 2.0 mW kg^{-1} in the troposphere, and 5.5 mW kg^{-1} in the stratosphere (not taking into account the tropopause region 1 km above and below the tropopause).

Model simulations for the BEXUS 8 flight interpolated to the flight trajectory are plotted in the left panel of Figure 3. Again, the agreement with the observations is excellent. A snapshot for the middle of the ascent isare presented in Figure 4. Tropo-

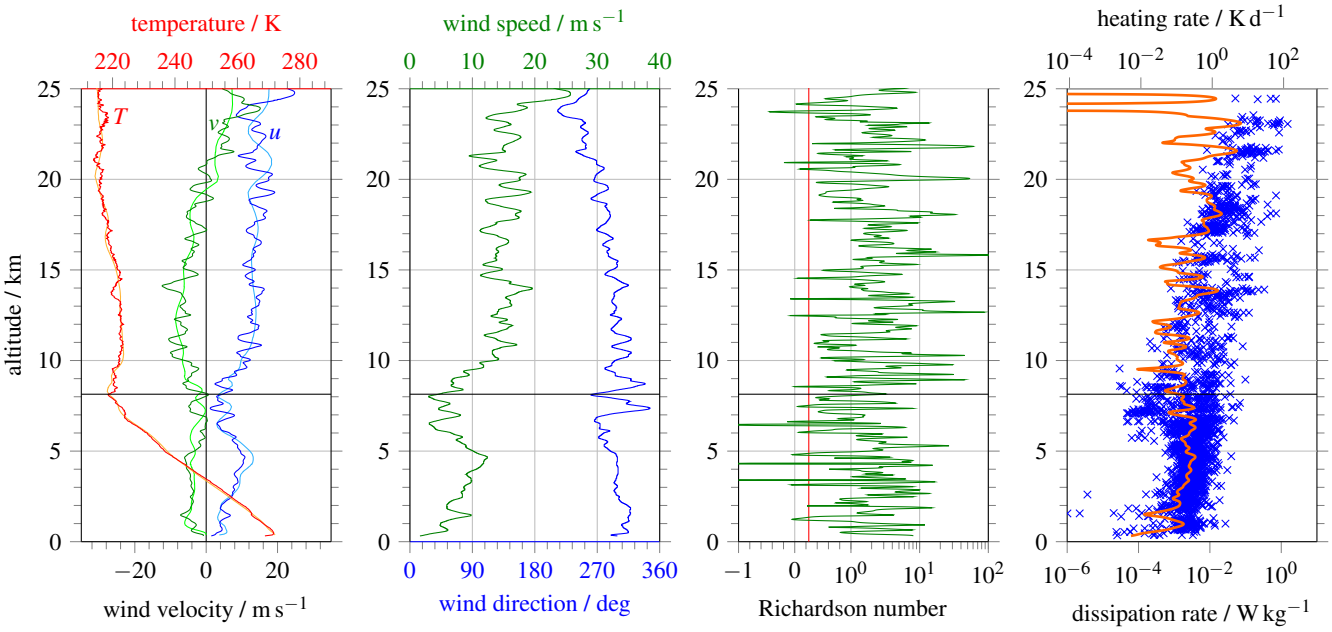

Figure 3. Same as Figure 1, but for the BEXUS 8 flight (10 Oct 2009)

spheric winds flowed against the Scandinavian mountains from western directions, but were weaker than during BEXUS 12. No jet was present. The expected mountain waves are visible in the vertical winds. In the lee of the mountains, wave patterns with smaller amplitudes are present at the location of the flight track. They intensify above altitudes of ∼20 km. No drop in wave amplitude similar to that during BEXUS 12 at ∼10 km is visible. This is consistent with no wave filtering and moderate dissipation rates throughout all altitudes with no peak in dissipation during BEXUS 8. The model TKE shows no enhancement outside the boundary layer, consistent with no wave filtering and no pronounced maximum in dissipation.

3.3 The 27 March 2014 flight

A small LITOS payload of second generation was launched from Kühlungsborn aton 27 Mar 2014, at 10:10 UT.

The left panel of Figure 5 shows temperatures smoothed over 15 data points (∼150 m) as well as zonal and meridional winds. The smoothing is necessary because for this flight the temperature measurement is perturbed by radiation effects as the radiosonde was incorporated in the main payload; these effects get worse with increasing altitude. Temperatures decreased up to the tropopause at 9 km. Between 9 km and ∼30 km altitude they stayed nearly constant and started to increase further upwards. Winds were easterly and turned northerlywards above ∼20 km altitude. A strong southeasterly jet was present between ∼6 km and 10 km height. Superposed are signatures of small-scale gravity waves. Wind shears originating from the jet may have excited turbulence and/or waves. The effect of the shear is visible as a layer with enhanced dissipation at this altitude (see

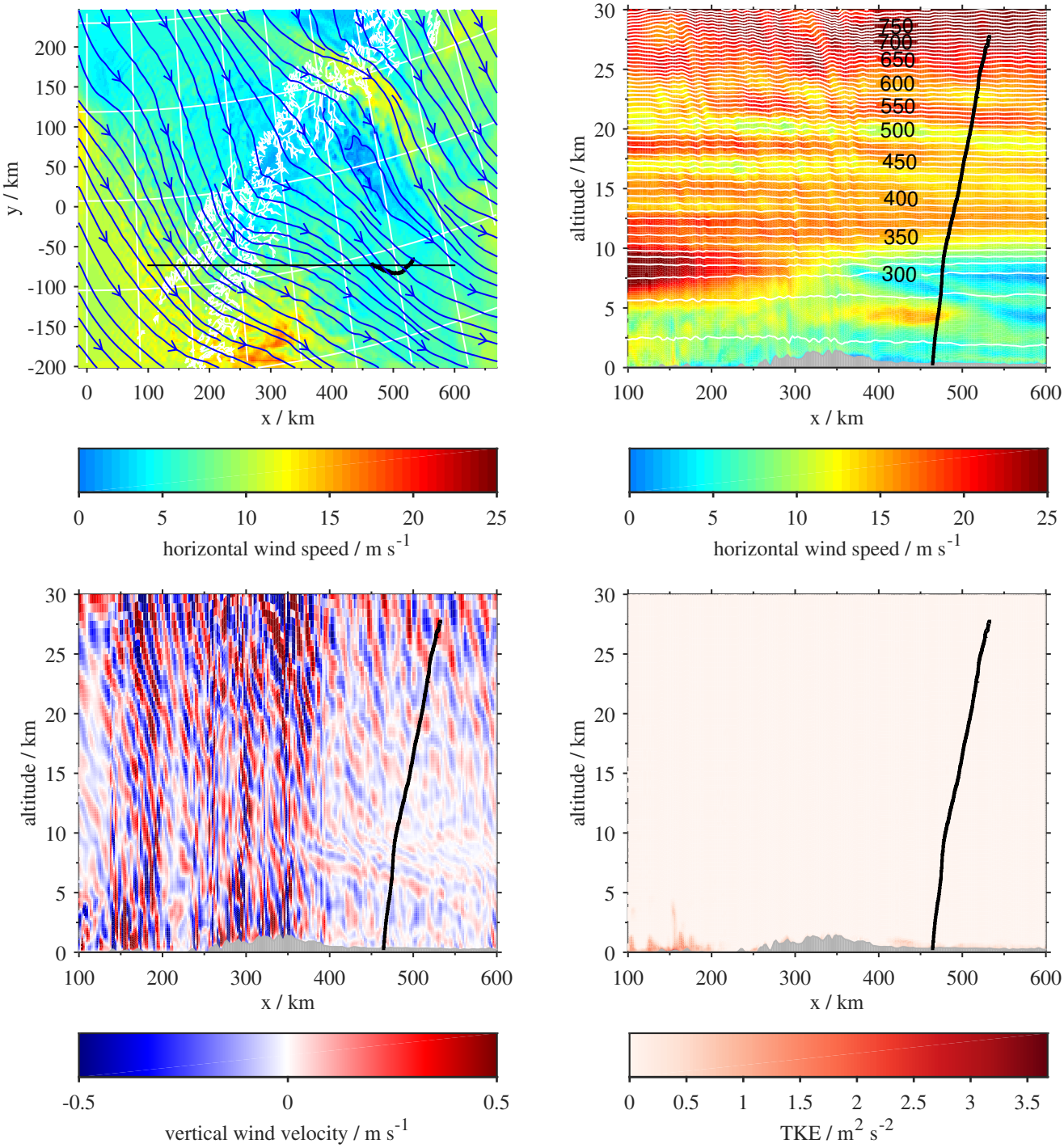

Figure 4. Same as Figure 2, but for WRF simulations for 10 Oct 2009, 9:00 UT and showing the trajectory of the BEXUS 8 flight. Please note that for the TKE the colourbar is scaled differently than in Figure 2.

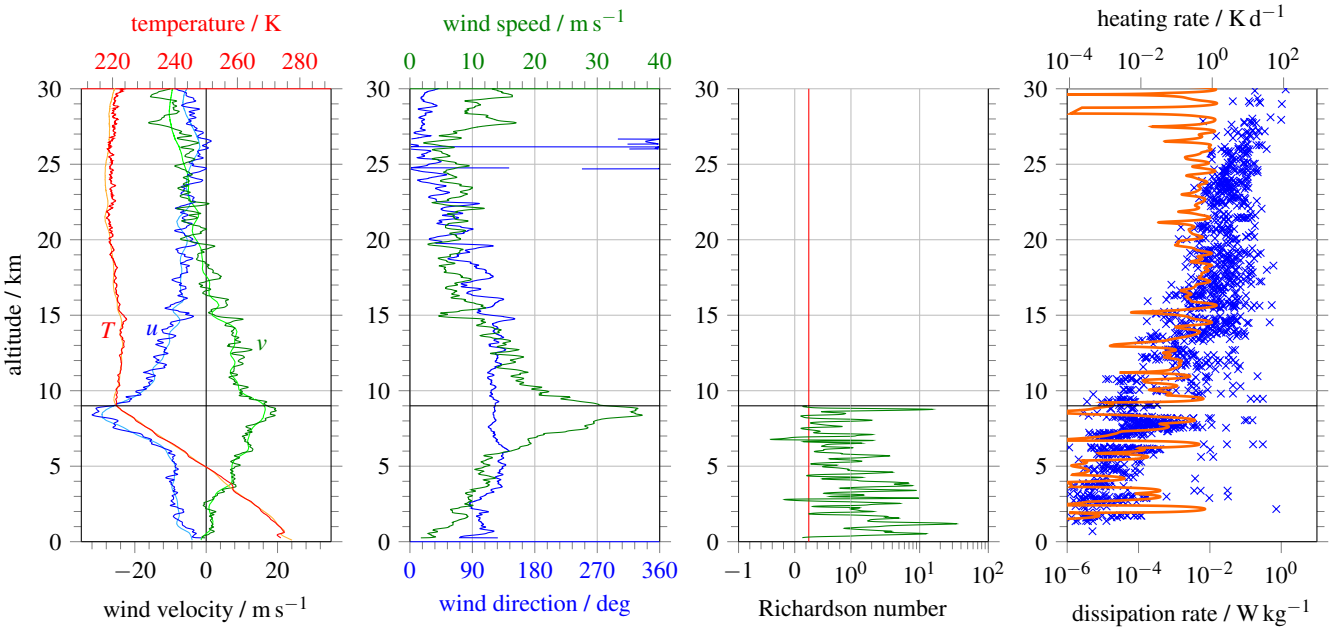

Figure 5. Same as Figure 1, but for the flight from Kühlungsborn at 27 Mar 2014. Due to disturbances of the temperature data, temperatures are smoothed in the plot in the left panel, and Richardson numbers are shown only for altitudes lower than 9 km. The dissipation profile excludes the lowermost 650 m due to disturbances from the launch procedure (dereeling of the payload suspension).

below). Richardson numbers are shown for altitudes below 9 km only because they involve derivatives of the temperature profile which was disturbed by radiation effects as described above.

Dissipation rates are presented in the right panel of Figure 5. The data below 650 m altitude are affected by the launch procedure (precisely the unwinding of the dereelers) and are thus discarded and not shown in the plot. ε values show the well-known intermittency similar to the BEXUS flights. The running average shows some structure in the troposphere, e. g. a few layers that are standing out with larger rates. Most prominently this can be seen near 8 km. That is in the same altitude as the wind shear due to the jet, which speaks for shear-induced turbulence. Precisely, there were two turbulent layers from 7.5 km to 7.9 km and from 8.1 km to 8.3 km height; within both, Richardson numbers were below 1 and partly below 1/4. Other sheets with large dissipation were, e. g., near 6.1 km and around 3.0 km altitude. In the lower stratosphere dissipation rates increased with altitude, while the variation was smaller compared to the troposphere. Mean values are 0.50 mW kg^{-1} in the troposphere and 4.0 mW kg^{-1} in the stratosphere.

To validate the corresponding WRF simulations, winds and temperatures interpolated to the flight track are plotted in the left panel of Figure 5. They agree very well to the radiosonde data. Figure 6 depicts WRF results from WRF simulations for the time of the flight. The upper left panel shows horizontal winds at 850 hPa, which were easterly or south-easterly. In the upper right panel horizontal winds are depicted as altitude section, showing that the strong jet had not much structure in horizontal direction, while the sharp vertical structure is reproduced as observed by the radiosonde. The lower left panel shows a vertical

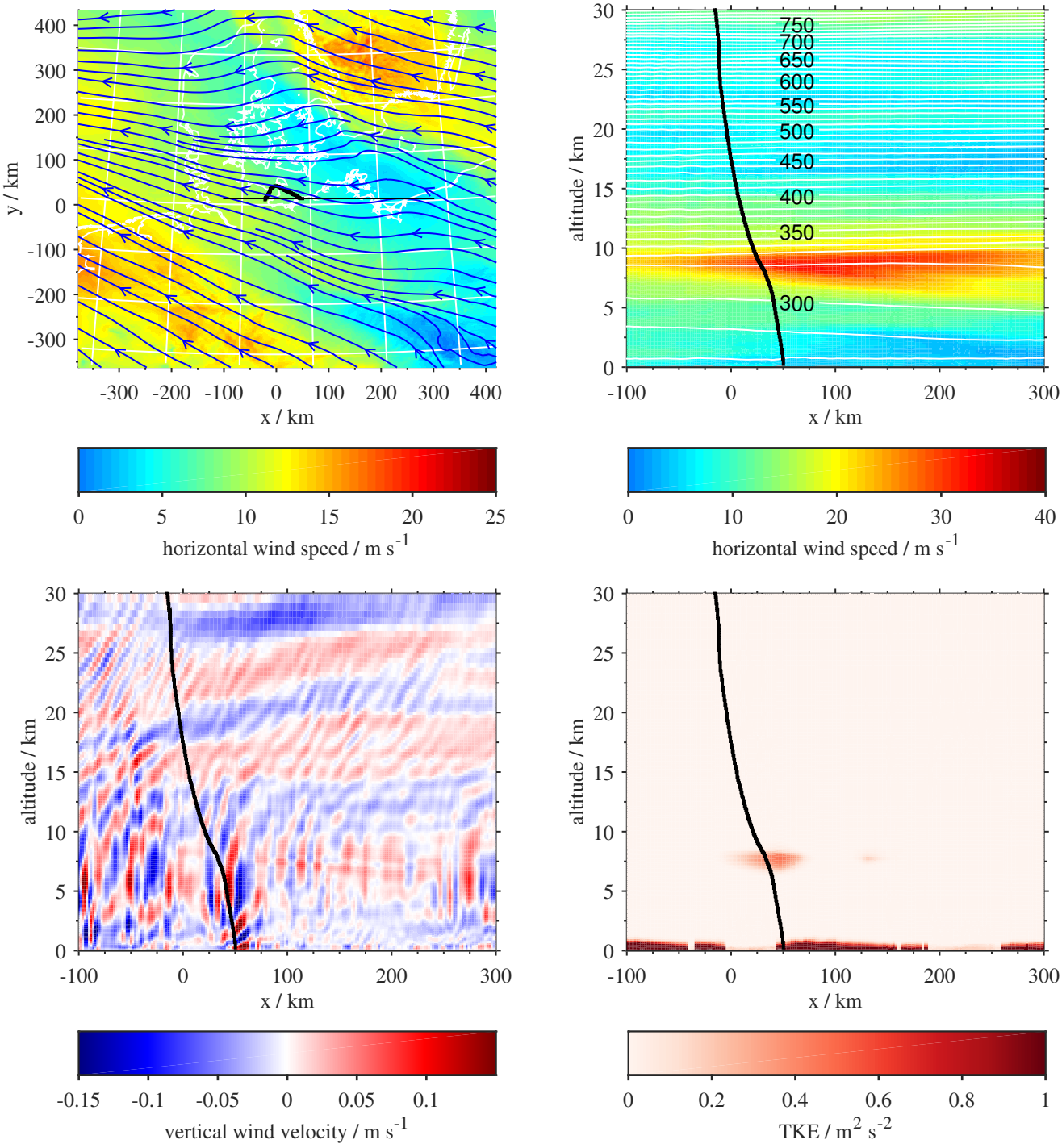

Figure 6. Same as Figure 2, but for WRF simulations for 27 Mar 2014, 11:00 UT.

profile of vertical winds. Wave patterns are visible, which stretch over the whole altitude range. Particularly, a superposition of a wave with long vertical wavelength ($\lambda_z \approx 8$ km) and nearly horizontal phase fronts and waves with short horizontal wavelength (10 km to 20 km) and phase fronts in the vertical can be seen. The occurrence of wave patterns corresponds to medium energy dissipation observed throughout all altitudes. The lower right panel of Figure 6 shows the TKE. Outside the boundary layer there is an enhancement near 7.5 km altitude. It corresponds nicely to a thick, strong turbulent layer in the measurement by LITOS between ~7 km and 8.5 km height. Within this observed turbulent layer, which in fact consists of several layers, Richardson numbers are smaller than 1 almost everywhere and partly evenat times smaller than 1/4.

3.4 The 11/12 July 2015 flight

A night-time flight with LITOS was performed aton 11/12 Jul 2015 from Kühlungsborn, launched at midnight local time (22:01 UT aton 11 Jul). The radiosonde was positioned 60 m below the main payload to avoid disturbances of the temperature sounding. The observed background parameters are depicted in the two left panels of Figure 7. Westerly winds prevailed up to ~19 km altitude, whereas above winds came from the east. This change in direction was not associated with a significant wind shear because velocities were small in that altitude region. A jet is visible at about 10 km height. Superposed on the winds are signatures of small-scale gravity waves. Above the tropopause at 11.3 km altitude there was a small tropopause inversion layer. Higher up temperatures remained rather constant up to ~20 km, where they started to increase.

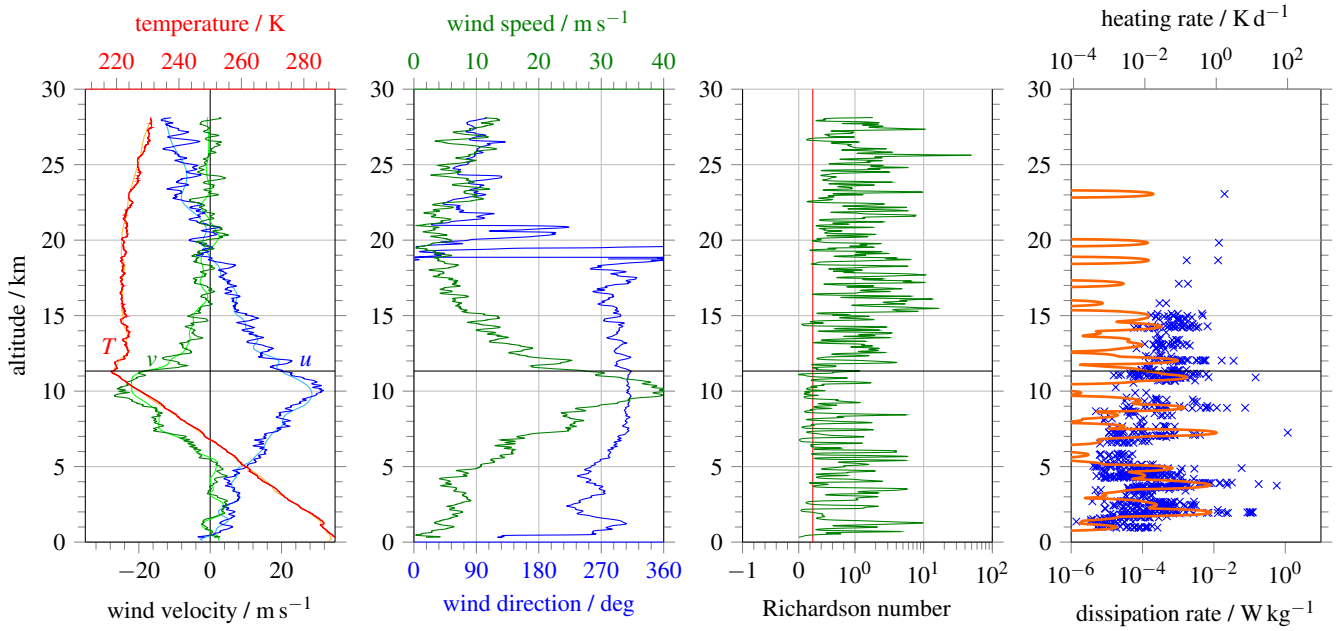

Figure 7. Same as Figure 1, but for the flight from Kühlungsborn at 11/12 Jul 2015. The dissipation profile excludes the lowermost 550 m due to disturbances from the launch procedure (dereeling of the payload suspension).

Richardson numbers were typically lower than for the other flights, indicating less stability. There are several layers where the Richardson number is below the critical limit of Ri_c (1/4). These layers are relatively thin.

Energy dissipation rates (data below 550 m are excluded due to disturbances from the launch procedure) showed a strong layerpatchy structure, with enhanced dissipation at, e. g., ∼2.0 km, 3.8 km, 7.2 km, 8.9 km, 11.0 km, 12.1 km, and 14.3 km. These layers of intense turbulence mostly corresponded to Richardson numbers smaller than $Ri_c = 1/4$, or at least to $Ri < 1$. Above ∼15 km altitude, hardly any turbulence was detected; only a few thin turbulent layers were observed. Thus above 15 km the average dissipation rate (for which no turbulence is counted as zero) was only 0.01 mW kg^{-1}, while below 15 km it was 0.64 mW kg^{-1}.

Results from corresponding WRF simulations are depicted in Figure 8. Horizontal winds at the 850 hPa level were mainly westerly. The altitude section shows that the strong jet did not have much variation in the horizontal direction. Vertical winds reveal wave patterns that are particularly intense around the tropopause and gradually become weaker near ∼15 km, with less amplitude above. This drop in wave amplitude is at the same altitude as the drop in observed dissipation. The TKE has enlarged values around 3 km altitude and near the tropopause, however the enhancement is small at the flight path. Correspondingly, the thickness of the strong turbulent layers detected by LITOS is relatively small; that means that these dissipative layers are potentially not resolved in the model.

4 Discussion

A comparison of the observed dissipation profiles and the wave patterns in the model vertical winds for the different flights yieldssuggests that more turbulence observed by LITOS comes along with stronger wave patterns visible in WRF, and vice versa. Particularly, this can be seen at the BEXUS 12 flight (27 Sep 2011) at the jump in dissipation and wave amplitude at ∼10 km altitude. In this case, the involved mechanism is a shear instability and potential wave filtering shortly below. At 12 Jul 2015, average dissipation rates drop at ∼15 km height, and so does the wave amplitude visible in WRF. A similar feature has been observed during another flight at 06 Jun 2014 (not shown): Likewise, LITOS data exhibit a sharp drop in turbulence at ∼15 km, and the corresponding WRF simulation shows strong wave patterns below ∼15 km and very weak ones above. In contrast, the flights from 10 Oct 2009 and 27 Mar 2014 do not show such a drop in dissipation rate or wave amplitude. For these two flights, moderate dissipation rates as well as wave amplitudes continue throughout all altitudes, with a slight increase towards higher altitudes.

The relation between waves and turbulence can also be seen in averages over altitude regions. Table 1 summarises mean dissipation rates from LITOS and mean absolute vertical fluxes in WRF for the flights presented in Section 3. For 12 Jul 2015, average dissipation rates above 15 km are more than two orders of magnitude lower than for the other flights. Below 15 km, mean ε values are in the same order of magnitude for all flights. At 12 Jul 2015 average dissipation rates below and above 15 km deviate by nearly two orders of magnitude. Consistently, the average absolute vertical flux above 15 km is lowest for all flights, and the values below and above 15 km deviate by one order of magnitude. At 27 Mar 2014 the fluxes below and above

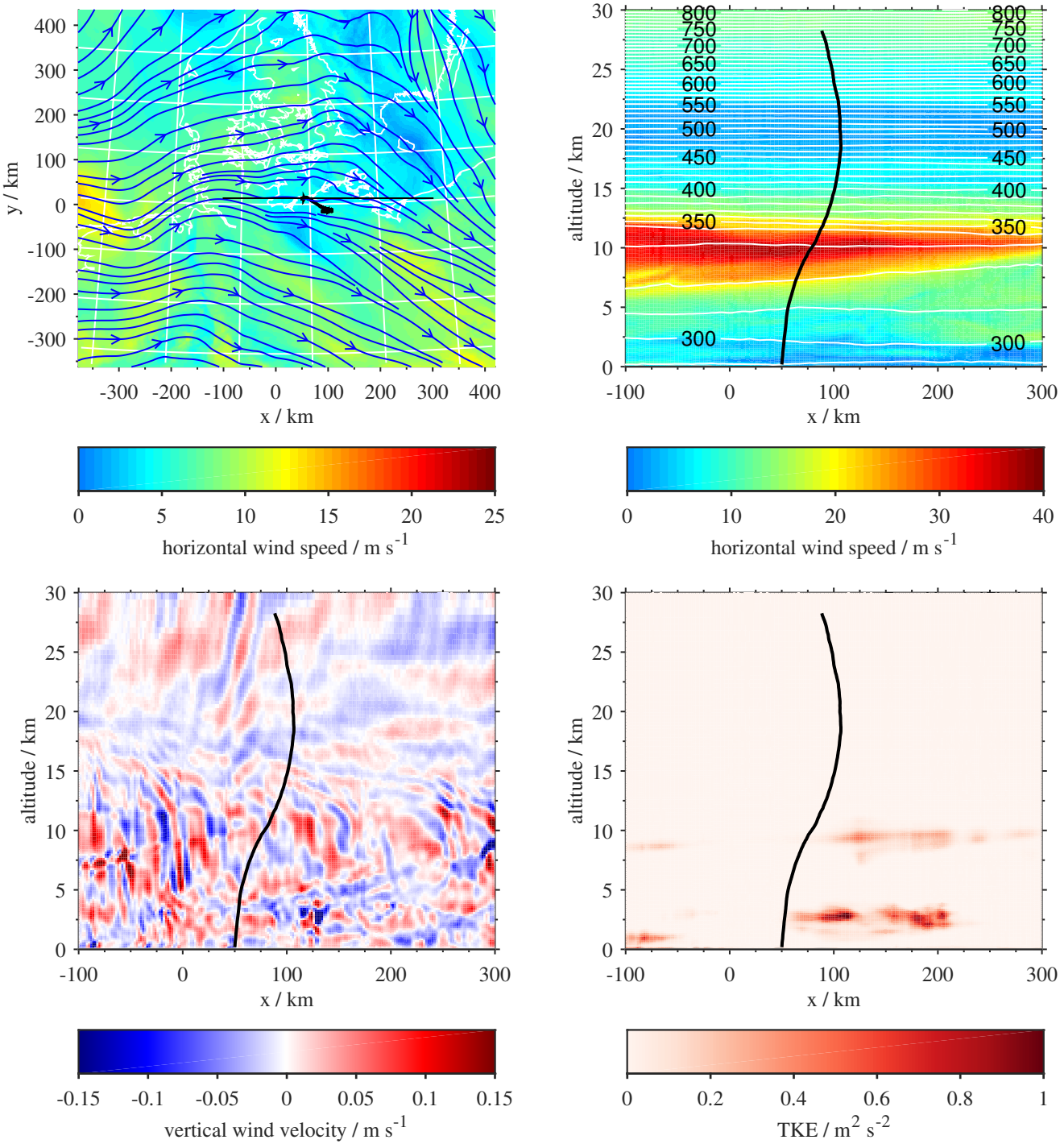

Figure 8. Same as Figure 2, but for WRF simulations for 11 Jul 2015, 23:00 UT

Table 1. Average dissipation rates observed by LITOS and mean absolute values of vertical energy fluxes from the WRF model. The fluxes are taken from a y section through the launch point averaged over the x coordinate in an area 50 km east and west of the launch point and over altitude from 7.5 km to 12.5 km (< 15 km) or 17.5 km to 22.5 km (> 15 km).

Flight		mean dissipation rate / mW kg^{-1}					mean vert. flux / W m^{-2}	
Date	Place of launch	tropo	strato	all	< 15 km	> 15 km	< 15 km	> 15 km
10 Oct 2009	Kiruna	2.0	5.5	4.4	2.1	6.9	0.18	0.073
27 Sep 2011	Kiruna	2.7	3.5	3.5	3.0	4.2	0.23	0.028
27 Mar 2014	Kühlungsborn	0.50	4.0	3.1	1.1	4.6	0.038	0.015
12 Jul 2015	Kühlungsborn	0.85	0.02	0.34	0.64	0.01	0.064	0.0069

15 km only deviate by a factor of 2.5. For the BEXUS flights (10 Oct 2009 and 27 Sep 2011), both dissipation rates and fluxes are on average larger than for the flights from Kühlungsborn (27 Mar 2014 and 12 Jul 2015).

We interpret this behaviour as continuous partial wave breaking the effect of wave saturation., meaning that a wave continuously loses amplitude by transferring energy to smaller scales and eventually turbulence due to non-linear processes. As described in the introduction, a saturated wave looses part of its energy to turbulence so that the amplitude does not grow further. Such effects have already been observed, e. g., by Cot and Barat (1986), who measured a gravity wave with almost constant amplitude over an altitude range of 5 km and collocated isolated turbulent patches with a dissipation rate approximately accounting for the energy loss of the wave. Partial wave breaking has been observed by lidar and described by Franke and Collins (2003). They found regions of strong overturning, and upwards propagating waves present below as well as (with less amplitude) above the overturning region. They argue that, depending on the amplitude, a breaking wave is not always completely annihilated, but the amplitude may be modulated in a highly non-linear event. Nappo (2002, p. 125) states that "gravity wave and turbulence are often observed to exist simultaneously." Via the process of continuous wave breaking, the occurrence of waves is connected to the intensity of turbulence. Pavelin et al. (2001) observed intense turbulence in the lowermost stratosphere during a period of maximal wave intensity using radar at Aberystwyth (52.4° N, 4.0° W), which supports the above hypothesis.

Saturation theories proposed several mechanisms, e. g. linear instability dynamics due to large wave amplitudes, non-linear damping, or non-linear wave-wave interactions (Fritts and Alexander, 2003, Section 6.3). The present study cannot answer that debate, yet the relatively large Richardson numbers hint that non-linear interactions may play a role.

Mean dissipation rates observed by LITOS are in the order of 10^{-3} W kg^{-1} (roughly 0.1 K d^{-1}). This is an order of magnitude below typical solar or chemical heating rates which are in the order of 1 K d^{-1} (Brasseur and Solomon, 1986, Fig. 4.19b). However, within thin layers rates of 10^{-1} W kg^{-1} ($\sim$10 K d^{-1}) are observed, which is larger than solar heating. The low mean energy dissipation rates are not explicitly contained even in high-resolution models, which cannot describe the large intermittency. Only large layers with highly increased dissipation as encountered during BEXUS 12 are captured.

Observed dissipation rates are partly larger than those reported by other publications using different methods. Barat (1982) obtained values between 1.4×10^{-5} W kg^{-1} and 3.9×10^{-5} W kg^{-1} from balloon measurements. Wilson et al. (2014) found ε

values between $3 \times 10^{-5}\,\mathrm{W\,kg^{-1}}$ and $6 \times 10^{-4}\,\mathrm{W\,kg^{-1}}$ in the upper troposphere from radar measurements. These are lower rates than the averages in this work, but within the range of the variability. Lilly et al. (1974) observed stratospheric dissipation rates between $7 \times 10^{-4}\,\mathrm{W\,kg^{-1}}$ and $2 \times 10^{-3}\,\mathrm{W\,kg^{-1}}$, depending on the underlying terrain, with aircraft. These results are in similar order of magnitude as the averages in this study. Haack et al. (2014) reported mean dissipation rates of $2 \times 10^{-2}\,\mathrm{W\,kg^{-1}}$ for the BEXUS 6 balloon flight and $5 \times 10^{-3}\,\mathrm{W\,kg^{-1}}$ for BEXUS 8 for the altitude range 7 km to 26.5 km, using a slightly different retrieval. That their average value for BEXUS 8 is similar to the one in this study is a consequence of two compensating effects: The new retrieval with more rigorous quality control criteria yields more spectra classified as non-turbulent which contribute to the average with $\varepsilon = 0$, yet the updated value of the constant c_{l_0} in Equation (1) (cf. Appendix A) yields higher dissipation rates by a factor of $\sim$50 for the same l_0.

5 Conclusions

In this paper high-resolution turbulence observations with LITOS are complemented by model simulations with WRF to study the relation between turbulence, waves, and background conditions. Four flights are selected where in each case data from two wind sensors are available; this allows a high quality assurance.

Enhanced energy dissipation rates were observed where pronounced instabilities were detected by the radiosonde. Moreover, measured shear instabilities and associated enhancements in dissipation on scales resolved by WRF also coincide with enlarged model turbulent kinetic energies (TKE). For instance, during the BEXUS 12 flight (27 Sep 2011), a wind reversal was observed which caused a large shear instability (indicated by Richardson numbers smaller than 1/4) as well as potential wave filtering. The resulting turbulence was detected by LITOS as a region with strongly enhanced dissipation rate. The model turbulent kinetic energy (TKE) peaks in this region, highlighting the significance of that layer. When looking at the vertical winds from WRF, wave patterns change at that height with large amplitudes below and small ones above; this again suggests the occurrence of wave breaking. Thus in this case the geophysical cause of the observed turbulent layer is clearly visible. The large scale instability is resolved by the radiosonde and the model. On the other hand, many other (less intense) turbulent layers observed by LITOS are obviously too thin to be related to the much coarser data of the radiosonde or the WRF results.

A relation between turbulence detected by LITOS and the presence of wave-like structures in WRF is noted: For the available summer flights at 06 Jun 2014 (not shown) and 12 Jul 2015, hereafter scenario 1, a drop in turbulence occurrence at approximately 15 km altitude with hardly any turbulence above was observed. In contrast, no such feature was present at the other flights (scenario 2; 10 Oct 2009, 27 Sep 2011, and 27 Mar 2014), i. e. turbulence occurred at all altitudes. In the associated model simulations, wave signatures become weaker around 15 km for scenario 1 (06 Jun 2014 and 12 Jul 2015), while they continue throughout all altitudes for scenario 2 (the other flights). Altogether, observed dissipation generally is weaker during lower wave activity (as seen in WRF), and larger where larger wave amplitudes are seen. These findings can be explained by a continuous fractional wave breakingwave saturation.

Turbulence has been observed for Richardson numbers below as well as above the critical number of 1/4, partly even for values larger than 100. Such a violation of the classical theory by Miles (1961) and Howard (1961) has already been described

by several researchers, e. g. Achatz (2005); Galperin et al. (2007); Haack et al. (2014). Hines (1988) recognised the limitation of considering only vertical instability (as done when using the Richardson number) and proposed a concept of slantwise instabilities as created by gravity waves. He showed that turbulence is more likely to develop via slanted instability compared to vertical instability. Thus turbulence for $Ri > 1/4$ is comprehensible.

The above hypothesis is maderesults are based on the limited dataset from a few flights. More flights at selected meteorological situations are planned to further study such a connectionthe relation between waves and turbulence. Moreover, a direct measurement of gravity wave activity in combination to the turbulence observations is preferable.

Appendix A: Derivation of the constant c_{l_0} in Equation (1)

To retrieve energy dissipation rates from observed spectra, relation (1) between inner scale l_0 and dissipation rate ε, $\varepsilon = c_{l_0}^4 \nu^3 / l_0^4$, and especially the value of the constant c_{l_0} is important. To obtain correct values, care has to be taken of which component(s) of the spectral tensor are observed. In the following, the derivation of the constant c_{l_0} is summarised.

In the inertial subrange, the longitudinal component, transversal component, and trace of the structure function tensor for velocity fluctuations have the form

$$D_{xx}(r) = C_{xx} r^{2/3}, \tag{A1}$$

where xx is a placeholder for rr (longitudinal), tt (transversal), or ii (trace), and the structure constant has the form $C_{xx} = b_{xx} a_v^2 \varepsilon^{2/3}$ with $b_{\mathrm{rr}} = 1$, $b_{\mathrm{tt}} = \frac{4}{3}$, $b_{ii} = b_{\mathrm{rr}} + 2b_{\mathrm{tt}} = \frac{11}{3}$ (Tatarskii, 1971, p. 54ff) and the empirical constant $a_v^2 = 2.0$ (e. g. Pope, 2000, p. 193f). In the viscous subrange, the structure function is

$$D_{xx}(r) = \tilde{C}_{xx} r^2 \tag{A2}$$

with $\tilde{C}_{xx} = c_{xx} \frac{\varepsilon}{\nu}$ and the factors $c_{\mathrm{rr}} = \frac{1}{15}$, $c_{\mathrm{tt}} = \frac{2}{15}$, $c_{ii} = c_{\mathrm{rr}} + 2c_{\mathrm{tt}} = \frac{1}{3}$ (Tatarskii, 1971, p. 49).

Based on Heisenberg (1948, (28)), Lübken and Hillert (1992, (4)) gave a form of the temporal spectrum in the inertial and viscous subranges, which reads for velocity fluctuations

$$W(\omega) = \frac{\Gamma(\frac{5}{3}) \sin(\frac{\pi}{3})}{2\pi u_{\mathrm{b}}} C_{xx} \frac{(\omega/u_{\mathrm{b}})^{-5/3}}{\left(1 + \left(\frac{\omega/u_{\mathrm{b}}}{k_0}\right)^{8/3}\right)^2} \tag{A3}$$

where u_{b} is the ascent velocity of the balloon, $\Gamma(z) := \int_0^\infty t^{z-1} \mathrm{e}^{-t}\, \mathrm{d}t$ is the Gamma function, and k_0 denotes the breakpoint between inertial and viscous subrange. The normalisation is obtained by considering the limit $k \ll k_0$ for the inertial subrange. Using the relation $\Phi(k) = -\frac{u_{\mathrm{b}}^2}{2\pi k} \frac{\mathrm{d}W}{\mathrm{d}\omega}(k u_{\mathrm{b}})$ between temporal and spatial spectrum (Tatarskii, 1971, (6.14)), the corresponding three-dimensional spectrum is

$$\Phi_{xx}(k) = \frac{1}{6\pi} \frac{\Gamma(\frac{5}{3}) \sin(\frac{\pi}{3})}{2\pi} C_{xx} k^{-11/3} \frac{5 + 21\left(\frac{k}{k_0}\right)^{8/3}}{\left(1 + \left(\frac{k}{k_0}\right)^{8/3}\right)^3}. \tag{A4}$$

The constant c_{l_0} in (1) can be computed from the condition of the structure function at the origin

$$\frac{\mathrm{d}^2 D_{xx}}{\mathrm{d}r^2}(0) = \frac{8\pi}{3} \int_0^\infty \Phi_{xx}(k) k^4 \,\mathrm{d}k \tag{A5}$$

(Tatarskii, 1971, p. 49f). Inserting the structure function (A2) and the spectrum (A4) into condition (A5), integrating and solving for $1/k_0$ yields

$$l_0 = \frac{2\pi}{k_0} = \underbrace{2\pi \left(\frac{3}{16} \Gamma(5/3) \sin(\pi/3) \frac{b_{xx}}{c_{xx}} a_\mathrm{v}^2 \right)^{3/4}}_{=c_{l_0}} \left(\frac{\nu^3}{\varepsilon} \right)^{1/4}. \tag{A6}$$

CTA wire probes are sensitive perpendicular to the wire axis but insensitive parallel to the wire axis. For the earlier flights, the wires of the CTA sensors were oriented vertically so that they are sensitive in both horizontal directions and insensitive in the vertical direction, i. e. for an ascending balloon both transversal components are measured. Thus $b_{xx} = 4/3 + 4/3 = 8/3$ and $c_{xx} = 2/15 + 2/15 = 4/15$, which leads to $c_{l_0} = 14.1$. For the flight at 12 Jul 2015, one sensor with the wire oriented horizontally was flown, which is sensitive in the vertical and one horizontal direction yet insensitive in the other horizontal direction (parallel to the wire). In this case $b_{xx} = 1 + 4/3 = 7/3$ and $c_{xx} = 1/15 + 2/15 = 3/15$ so that $c_{l_0} = 15.8$.

Haack et al. (2014, Section 4) used different components of the structure function constant yielding $c_{l_0} = 5.7$. Since in (1) the constant occurs with $c_{l_0}^4$, this results in a difference in ε of a factor of $\sim$50 for the same l_0.

Acknowledgements. The data of the BEXUS 8 flight were kindly provided by Anne Haack. The BEXUS programme was financed by the German Aerospace Center (DLR) and the Swedish National Space Board (SNSB). We are grateful for the support by the "International Leibniz Graduate School for Gravity Waves and Turbulence in the Atmosphere and Ocean" (ILWAO) funded by the Leibniz Association (WGL). This study was partly funded by the German Federal Ministry for Education and Research (BMBF) research initiative "Role of the Middle Atmosphere In Climate" (ROMIC) under project numbers 01LG1206A and 01LG1218A (METROSI), and by the German Research Foundation (DFG) under project numbers LU 1174 (PACOG) and FOR 1898 (MS-GWaves). We thank Wayne K. Hocking and two anonymous reviewers for their valuable comments leading to the improvement of this article.

References

Achatz, U.: On the role of optimal perturbations in the instability of monochromatic gravity waves, Phys. Fluids, 17, doi:10.1063/1.2046709, 2005.

Andreassen, O., Wasberg, C. E., Fritts, D. C., and Isler, J. R.: Gravity wave breaking in two and three dimensions: 1. Model description and comparison of two-dimensional evolutions, J. Geophys. Res., 99, 8095–8108, doi:10.1029/93JD03435, 1994.

Balsley, B. B., Svensson, G., and Tjernström, M.: On the Scale-dependence of the Gradient Richardson Number in the Residual Layer, Bound.-Layer Meteor., 127, 57–72, doi:10.1007/s10546-007-9251-0, 2008.

Barat, J.: Some characteristics of clear-air turbulence in the middle stratosphere, J. Atmos. Sci., 39, 2553–2564, doi:10.1175/1520-0469(1982)039<2553:SCOCAT>2.0.CO;2, 1982.

Birner, T.: Fine-scale structure of the extratropical tropopause region, J. Geophys. Res., 111, D04 104, doi:10.1029/2005JD006301, 2006.

Birner, T., Dörnbrack, A., and Schumann, U.: How sharp is the tropopause at midlatitudes?, Geophys. Res. Lett., 29, 45–1–45–4, doi:10.1029/2002GL015142, 2002.

Brasseur, G. and Solomon, S.: Aeronomy of the middle atmosphere: chemistry and physics of the stratosphere and mesosphere, Atmospheric sciences library, Reidel, Dordrecht, 2nd edn., 1986.

Chen, F. and Dudhia, J.: Coupling an Advanced Land Surface–Hydrology Model with the Penn State-NCAR MM5 Modeling System. Part I: Model Implementation and Sensitivity, Mon. Wea. Rev., 129, 569–585, doi:10.1175/1520-0493(2001)129<0569:CAALSH>2.0.CO;2, 2001.

Cho, J. Y. N., Newell, R. E., Anderson, B. E., Barrick, J. D. W., and Thornhill, K. L.: Characterizations of tropospheric turbulence and stability layers from aircraft observations, J. Geophys. Res., 108, doi:10.1029/2002JD002820, 8784, 2003.

Chou, M. D. and Suarez, M. J.: An efficient thermal infrared radiation parameterization for use in general circulation models., NASA Tech. Memo., 104606, 85pp., 1994.

Clayson, C. A. and Kantha, L.: On Turbulence and Mixing in the Free Atmosphere Inferred from High-Resolution Soundings, J. Atmos. Oceanic Technol., 25, 833–852, doi:10.1175/2007JTECHA992.1, 2008.

Cot, C. and Barat, J.: Wave-turbulence interaction in the stratosphere: A case study, J. Geophys. Res., 91, 2749–2756, doi:10.1029/JD091iD02p02749, 1986.

Dalaudier, F., Sidi, C., Crochet, M., and Vernin, J.: Direct Evidence of "Sheets" in the Atmospheric Temperature Field, Journal of the Atmospheric Sciences, 51, 237–248, doi:10.1175/1520-0469(1994)051<0237:DEOITA>2.0.CO;2, 1994.

Ehard, B., Achtert, P., Dörnbrack, A., Gisinger, S., Gumbel, J., Khaplanov, M., Rapp, M., and Wagner, J. S.: Combination of lidar and model data for studying deep gravity wave propagation, Mon. Wea. Rev., 144, 77–98, doi:10.1175/MWR-D-14-00405.1, 2016.

Franke, P. M. and Collins, R. L.: Evidence of gravity wave breaking in lidar data from the mesopause region, Geophys. Res. Lett., 30, doi:10.1029/2001GL014477, 1155, 2003.

Fritts, D. C. and Alexander, M. J.: Gravity wave dynamics and effects in the middle atmosphere, Rev. Geophys., 41, doi:10.1029/2001RG000106, 2003.

Fritts, D. C. and Wang, L.: Gravity Wave–Fine Structure Interactions. Part II: Energy Dissipation Evolutions, Statistics, and Implications, J. Atmos. Sci., 70, 3735–3755, doi:10.1175/JAS-D-13-059.1, 2013.

Fritts, D. C., Wang, L., Geller, M. A., Lawrence, D. A., Werne, J., and Balsley, B. B.: Numerical Modeling of Multiscale Dynamics at a High Reynolds Number: Instabilities, Turbulence, and an Assessment of Ozmidov and Thorpe Scales, J. Atmos. Sci., 73, 555–578, doi:10.1175/JAS-D-14-0343.1, 2016.

Galperin, B., Sukoriansky, S., and Anderson, P. S.: On the critical Richardson number in stably stratified turbulence, Atmos. Sci. Let., 8, 65–69, doi:10.1002/asl.153, 2007.

Gavrilov, N. M.: Estimates of turbulent diffusivities and energy dissipation rates from satellite measurements of spectra of stratospheric refractivity perturbations, Atmos. Chem. Phys., 13, 12 107–12 116, doi:10.5194/acp-13-12107-2013, 2013.

Haack, A., Gerding, M., and Lübken, F.-J.: Characteristics of stratospheric turbulent layers measured by LITOS and their relation to the Richardson number, J. Geophys. Res., 119, 10 605–10 618, doi:10.1002/2013JD021008, 2014.

Hauf, T.: Aircraft Observation of Convection Waves over Southern Germany—A Case Study, Mon. Wea. Rev., 121, 3282–3290, doi:10.1175/1520-0493(1993)121<3282:AOOCWO>2.0.CO;2, 1993.

Heisenberg, W.: Zur statistischen Theorie der Turbulenz, Z. Phys., 124, 628–657, doi:10.1007/BF01668899, 1948.

Hines, C. O.: Generation of Turbulence by Atmospheric Gravity Waves, J. Atmos. Sci., 45, 1269–1278, doi:10.1175/1520-0469(1988)045<1269:GOTBAG>2.0.CO;2, 1988.

Hines, C. O.: The Saturation of Gravity Waves in the Middle Atmosphere. Part I: Critique of Linear-Instability Theory, J. Atmos. Sci., 48, 1348–1360, doi:10.1175/1520-0469(1991)048<1348:TSOGWI>2.0.CO;2, 1991.

Hocking, W. K.: A review of Mesosphere–Stratosphere–Troposphere (MST) radar developments and studies, circa 1997–2008, Journal of Atmospheric and Solar-Terrestrial Physics, 73, 848–882, doi:http://dx.doi.org/10.1016/j.jastp.2010.12.009, 2011.

Hodges, R. R.: Generation of turbulence in the upper atmosphere by internal gravity waves, J. Geophys. Res., 72, 3455–3458, doi:10.1029/JZ072i013p03455, 1967.

Hong, S.-Y. and Lim, J.-O. J.: The WRF single-moment 6-class microphysics scheme (WSM6), J. Korean Meteor. Soc., 42, 129–151, 2006.

Howard, L. N.: Note on a paper of John W. Miles, J. Fluid Mech., 10, 509–512, doi:10.1017/S0022112061000317, 1961.

Kain, J. S. and Fritsch, J. M.: A One-Dimensional Entraining/Detraining Plume Model and Its Application in Convective Parameterization, J. Atmos. Sci., 47, 2784–2802, doi:10.1175/1520-0469(1990)047<2784:AODEPM>2.0.CO;2, 1990.

Klemp, J. B., Dudhia, J., and Hassiotis, A. D.: An Upper Gravity-Wave Absorbing Layer for NWP Applications, Mon. Wea. Rev., 136, 3987–4004, doi:10.1175/2008MWR2596.1, 2008.

Lilly, D. K., Waco, D. E., and Adelfang, S. I.: Stratospheric Mixing Estimated from High-Altitude Turbulence Measurements, J. Appl. Meteor., 13, 488–493, doi:10.1175/1520-0450(1974)013<0488:SMEFHA>2.0.CO;2, 1974.

Lindzen, R. S.: Turbulence and stress owing to gravity wave and tidal breakdown, J. Geophys. Res., 86, 9707–9714, doi:10.1029/JC086iC10p09707, 1981.

Lübken, F.-J. and Hillert, W.: Measurements of turbulent energy dissipation rates applying spectral models, in: Coupling Processes in the Lower and Middle Atmosphere, pp. 345–351, NATO Advanced Research Workshop, Kluwer Press, Loen, Norway, 1992.

Luce, H., Fukao, S., Dalaudier, F., and Crochet, M.: Strong Mixing Events Observed near the Tropopause with the MU Radar and High-Resolution Balloon Techniques, J. Atmos. Sci., 59, 2885–2896, doi:10.1175/1520-0469(2002)059<2885:SMEONT>2.0.CO;2, 2002.

Miles, J. W.: On the stability of heterogeneous shear flows, J. Fluid Mech., 10, 496–508, doi:10.1017/S0022112061000305, 1961.

Mlawer, E. J., Taubman, S. J., Brown, P. D., Iacono, M. J., and Clough, S. A.: Radiative transfer for inhomogeneous atmospheres: RRTM, a validated correlated-k model for the longwave, J. Geophys. Res., 102, 16 663–16 682, doi:10.1029/97JD00237, 1997.

Nakanishi, M. and Niino, H.: Development of an Improved Turbulence Closure Model for the Atmospheric Boundary Layer, J. Meteor. Soc. Japan, 87, 895–912, http://ci.nii.ac.jp/naid/110007465760/en/, 2009.

Nappo, C. J.: An Introduction to Atmospheric Gravity Waves, vol. 85 of *International Geophysics Series*, Academic Press, San Diego, 2002.

Paoli, R., Thouron, O., Escobar, J., Picot, J., and Cariolle, D.: High-resolution large-eddy simulations of stably stratified flows: application to subkilometer-scale turbulence in the upper troposphere–lower stratosphere, Atmos. Chem. Phys., 14, 5037–5055, doi:10.5194/acp-14-5037-2014, 2014.

Pavelin, E., Whiteway, J. A., and Vaughan, G.: Observation of gravity wave generation and breaking in the lowermost stratosphere, J. Geophys. Res., 106, 5173–5179, doi:10.1029/2000JD900480, 2001.

Plougonven, R., Hertzog, A., and Teitelbaum, H.: Observations and simulations of a large-amplitude mountain wave breaking over the Antarctic Peninsula, J. Geophys. Res., 113, doi:10.1029/2007JD009739, d16113, 2008.

Pope, S. B.: Turbulent Flows, Cambridge University Press, Cambridge, 2000.

Schneider, A., Gerding, M., and Lübken, F.-J.: Comparing turbulent parameters obtained from LITOS and radiosonde measurements, Atmos. Chem. Phys., 15, 2159–2166, doi:10.5194/acp-15-2159-2015, 2015.

Skamarock, W. C., Klemp, J. B., Dudhia, J., Gill, D. O., Barker, D. M., Duda, M. G., Huang, X.-Y., Wang, W., and Powers, J. G.: A description of the Advanced Research WRF Version 3, NCAR technical note, Mesoscale and Microscale Meteorology Division, National Center for Atmospheric Research, Boulder, Colorado, USA, http://www2.mmm.ucar.edu/wrf/users/docs/arw_v3.pdf, 2008.

Tatarskii, V. I.: The effects of the turbulent atmosphere on wave propagation, Israel Program for Scientific Translations, Jerusalem, translated from Russian, 1971.

Theuerkauf, A., Gerding, M., and Lübken, F.-J.: LITOS – a new balloon-borne instrument for fine-scale turbulence soundings in the stratosphere, Atmos. Meas. Tech., 4, 55–66, doi:10.5194/amt-4-55-2011, 2011.

Wilson, R.: Turbulent diffusivity in the free atmosphere inferred from MST radar measurements: a review, Ann. Geophys., 22, 3869–3887, doi:10.5194/angeo-22-3869-2004, 2004.

Wilson, R., Luce, H., Hashiguchi, H., Nishi, N., and Yabuki, Y.: Energetics of persistent turbulent layers underneath mid-level clouds estimated from concurrent radar and radiosonde data, J. Atmos. Sol.-Terr. Phy., 118, Part A, 78–89, doi:10.1016/j.jastp.2014.01.005, 2014.

Worthington, R. M.: Tropopausal turbulence caused by the breaking of mountain waves, J. Atmos. Sol.-Terr. Phys., 60, 1543–1547, doi:10.1016/S1364-6826(98)00105-9, 1998.

Yamanaka, M. D., Tanaka, H., Hirosawa, H., Matsuzaka, Y., Yamagami, T., and Nishimura, J.: Measurement of Stratospheric Turbulence by Balloon-Borne "Glow-Discharge" Anemometer, J. Meteor. Soc. Japan Ser. II, 63, 483–489, https://www.jstage.jst.go.jp/article/jmsj1965/63/3/63_3_483/_article, 1985.